Work Package 6: Natural components of climate variability

This work package deals with the natural contributions to atmospheric variability. As climate change caused by anthropogenic influence has to be discriminated against natural effects a good knowledge of the related processes is a prerequisite for studying the coupled effects of dynamics and chemistry in the atmosphere. Within KODYACS, the influence of the solar cycle, volcanic eruptions and the quasi biennial oscillation (QBO) on the state of the atmosphere are studied on different methodical levels: observations, process studies, CCM-sensitivity studies and CCM transient runs.

Contribution of IMK-MIPAS

Observations related to solar variability and state of the upper atmosphere: Development of the upper stratospheric/mesospheric/thermospheric temperature, ozone, NO_2, NO, and CO retrieval

This activity contributes to the question to which part individual components of natural variability (in particular solar activity cycles) contribute to the observed changes of trace gases and meteorological variables. It was planned to do this by comparing MIPAS/ENVISAT data on the distribution of stratospheric ozone, NO, temperature and others with simulations of the KASIMA model, in order to study the impact of solar events on the state of the stratosphere. Moreover, mesospheric distributions of ozone and the temperature derived from MIPAS/ENVISAT data can be used to better understand the energy budget of this atmospheric region as well as its reaction on solar activity, and to provide upper boundary condition for KASIMA. Specific algorithms to account for so-called non-LTE effects in the population of molecular states have been developed for this purpose together with our co-operation partner Instituto de Astrofísica de Andalucía (IAA/CSIC). These algorithms have been implemented in our radiative transfer/retrieval processing system KOPRA-RCP.

The development of retrieval methods has to distinguish between: 1) retrieval of upper stratospheric and mesospheric distributions from data of the standard observation mode (6 – 68 km altitude); 2) retrieval of upper stratospheric to thermospheric distributions from the so-called “Upper Atmosphere” modes, which cover the atmosphere up to 150 km. The latter observation scenarios, however, were run so far only for a few orbits in July 2002 and June 2003. For this reason, most of the material presented here focusses on the retrieval of trace gas and temperature distributions in the upper stratosphere and mesosphere from the standard observation scenario.

Funded from resources external to this project, the generalised non-LTE model GRANADA has been developed which is currently applicable to 10 trace species in the atmosphere (Funke et al., 2002). Within this model the non-LTE state population for the actual atmospheric situation (kinetic temperature profile, distribution of various trace species, solar zenith angle, solar activity etc.) can be calculated. In particular, this model describes the population of the molecular states of NO, CO, NO_2, O_3, CO_2, CH_4, H_2O and others.

As a contribution to KODYACS, the generalised non-LTE model GRANADA has been included in our radiative transfer model KOPRA (Stiller et al., 2002) which is part of the scientific level-2 data processor at IMK. Besides the population of the molecular states, GRANADA provides the derivatives of the measured radiance spectrum with respect to certain non-LTE process parameters.

The approach to retrieve simultaneously the vmr of species like NO or O_3 together with non-LTE process parameters has been developed on basis of the generalised non-LTE model, the radiative transfer model KOPRA, and the retrieval algorithm RCP, which build the kernel of the IMK data processor. The various approaches to non-LTE retrieval built in the processor are described in detail in (von Clarmann et al., 2003a, and López-Puertas et al., 2002a).

Regarding the NO retrieval and the achievable performance, the specification of a baseline had been reached before the start of the KODYACS project (see, Funke et al., 2000; 2001). Therefore it is not described here.

For the improved O_3 vmr retrieval in the upper stratosphere and mesosphere, a micro window selection concentrating on the 10 µm region of the spectral data has been performed. This spectral region is very strongly influenced by non-LTE effects and therefore excluded in the operational data processing. The strong signals there, however, can favourably be used to improve the retrieval performance if proper non-LTE modelling is achieved. The non-LTE processes to be considered in the non-LTE retrieval of the O_3

vmr from the MIPAS spectra are chemical excitation, V-V and V-T relaxation rates, and losses in chemical re-combination which are modelled for the 105 lowest vibrational energy levels. All processes depend on the O_3 vmr itself. Therefore, in each iteration step of the retrieval, the population of the molecular states are re-calculated according to the current O_3 vmr.

The retrieval of temperature in the standard observation mode from 6 to 68 km altitude is done simultaneously with the line-of-sight (LOS) pointing retrieval. The method and its application to first MIPAS data is published in (von Clarmann et al., 2003b). This approach which assumes CO_2 to be in LTE is shown to be valid up to about 60 km except for the very warm polar night mesosphere. Temperatures retrieved under consideration of non-LTE are cooler than those retrieved under LTE by 1 to 2 K for daytime around 70 km and warmer by 3 to 7 K for polar night conditions (see Fig. WP6-1-1). These results are in agreement with expectations (von Clarmann et al., 2003b).

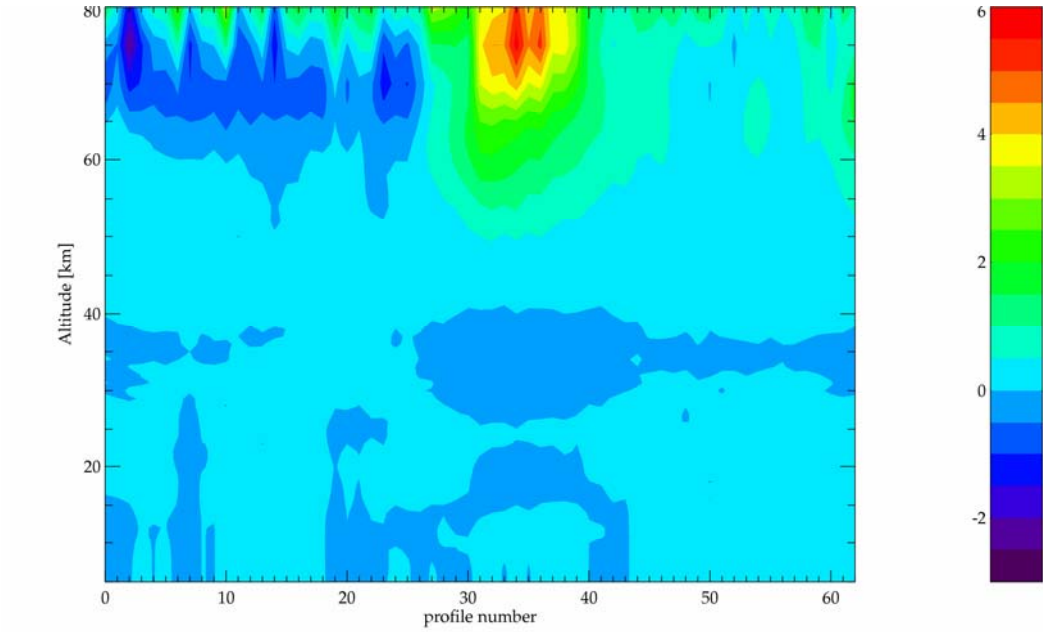

Fig. WP6-1-1: Differences in the temperature field retrieved from orbit no. 504 data (measured on April 5, 2002) from non-LTE and LTE retrieval approaches. Profiles no. 1 to 32 were measured under daytime conditions where non-LTE effects in mesospheric temperature are pronounced; the real temperature there is colder than the one retrieved under neglect of non-LTE. The south polar mesosphere (close to scan no. 32) is warmer than retrieved under neglect of non-LTE.

For the upper atmosphere observation modes a non-LTE retrieval scheme for simultaneous retrieval of temperature and CO_2 was developed. Small spectral intervals, so-call microwindows were selected in the 15 µm region (see Fig. WP6-1-2) from the fundamental band and the hot bands, near 10 µm, and at 4.3 µm. The information on temperature comes mainly from the 15 µm region at lower altitudes and from the 4.3 µm region at upper altitudes. Full modelling of population of CO_2 molecular states under non-LTE is included by using GRANADA. For more details see (López-Puertas et al., 2003b).

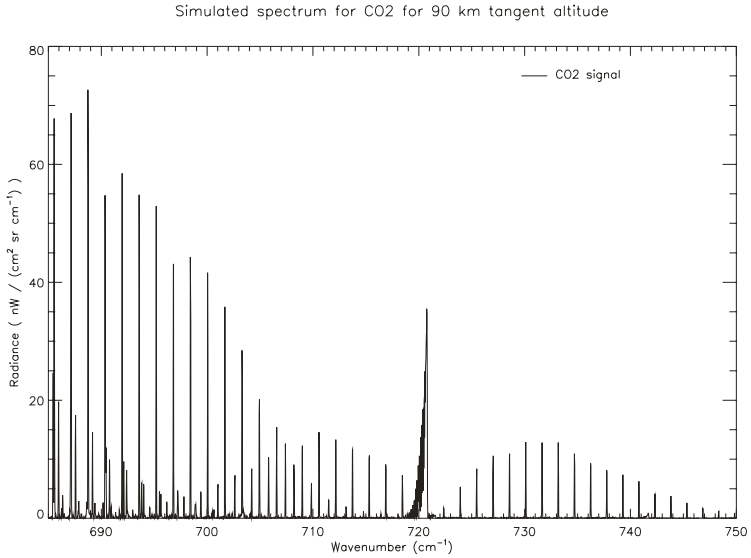

Fig. WP6-1-2: Simulated MIPAS spectrum for 90 km tangent altitude showing signatures of CO_2; the strong signatures on the left side decreasing to higher wave numbers belong to the CO_2 fundamental band and are used for the retrieval of kinetic temperature. The expected NESR in this spectral region is about 15 W/(sr cm^2) cm^{-1}.

First retrievals based on real data

MIPAS was successfully launched on the ENVISAT satellite on 1st March 2002. First spectral data of the atmosphere were measured on 24th March 2002. Since then the commissioning or calibration/validation phase was ongoing until October 2003. Its objectives were to characterise the instrument performance and to validate and improve the algorithms for deriving trace gas distributions and other atmospheric parameters from the raw data. As part of this it was validated that non-LTE effects can be disregarded in the operational retrieval for the temperature and 6 key species O_3, H_2O, N_2O, CH_4, HNO_3, and NO_2 in the stratosphere (López-Puertas et al., 2003a). Complementary to this, we investigated how far the altitude range in which sensible retrievals are possible can be extended if non-LTE effects are taken into account, and which information can be obtained. A limited amount of data was provided to us during the commissioning phase for the calibration/validation activities and functionality tests of our processor; these data, however, are not approved by ESA for scientific use.

Algorithms to derive temperature, ozone, NO, and other trace gases in the middle to upper atmosphere from MIPAS/ENVISAT data by accounting for non-LTE effects have been developed further taking into account and adjusting to real level-1b data quality (Stiller et al., 2003). Temperature and ozone vmr fields were retrieved from orbit 504 data (measured on 5 April 2002). Microwindows as selected for pure LTE retrieval, however, were used. Even then, compared to results of a LTE retrieval, the retrieved temperature (see Fig. WP6-1-1) and ozone fields (see Fig. WP6-1-3) show significant deviations above the stratopause region (up to 6 K in temperature and more than 7 % in ozone vmrs) while below the stratopause the LTE approach seems to achieve comparable results (López-Puertas et al., 2002b). This result confirms that the LTE approach is reasonable for retrievals in the stratosphere, however accounting for non-LTE is necessary to derive correct temperature and vmr fields in the stratopause region and above from MIPAS data.

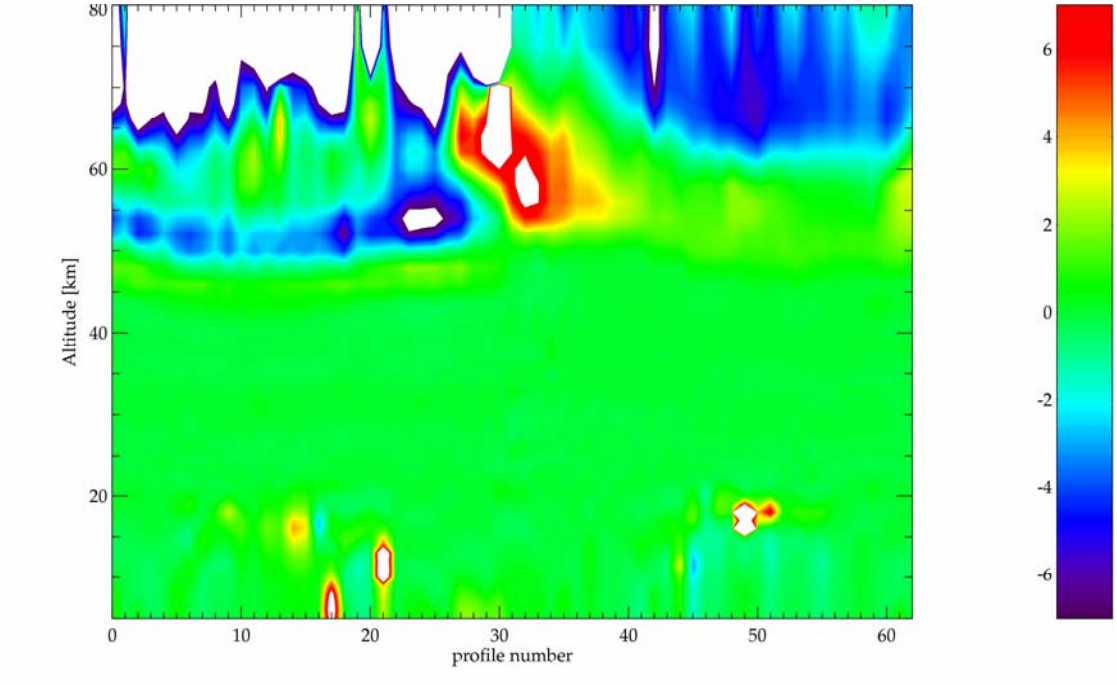

WP6-1-3: Differences in the ozone field (in ppmv) retrieved from orbit no. 504 data from non-LTE and LTE retrieval approaches; for the non-LTE retrieval approach the populations of the molecular states were updated according to the actual conditions in each iteration step. For more details, see text.

As a next step, the retrieval approaches were applied to MIPAS data measured in the "Upper Atmosphere" observation mode. Micro-windows selected for non-LTE retrieval were used for ozone (see Fig. WP6-1-4) (Gil-López et al., 2003) and temperature (see Fig. WP6-1-5). In case of O_3 retrieval, non-LTE effects were considered for CO_2, too, besides ozone, since the micro-windows contain CO_2 lines to a significant amount.

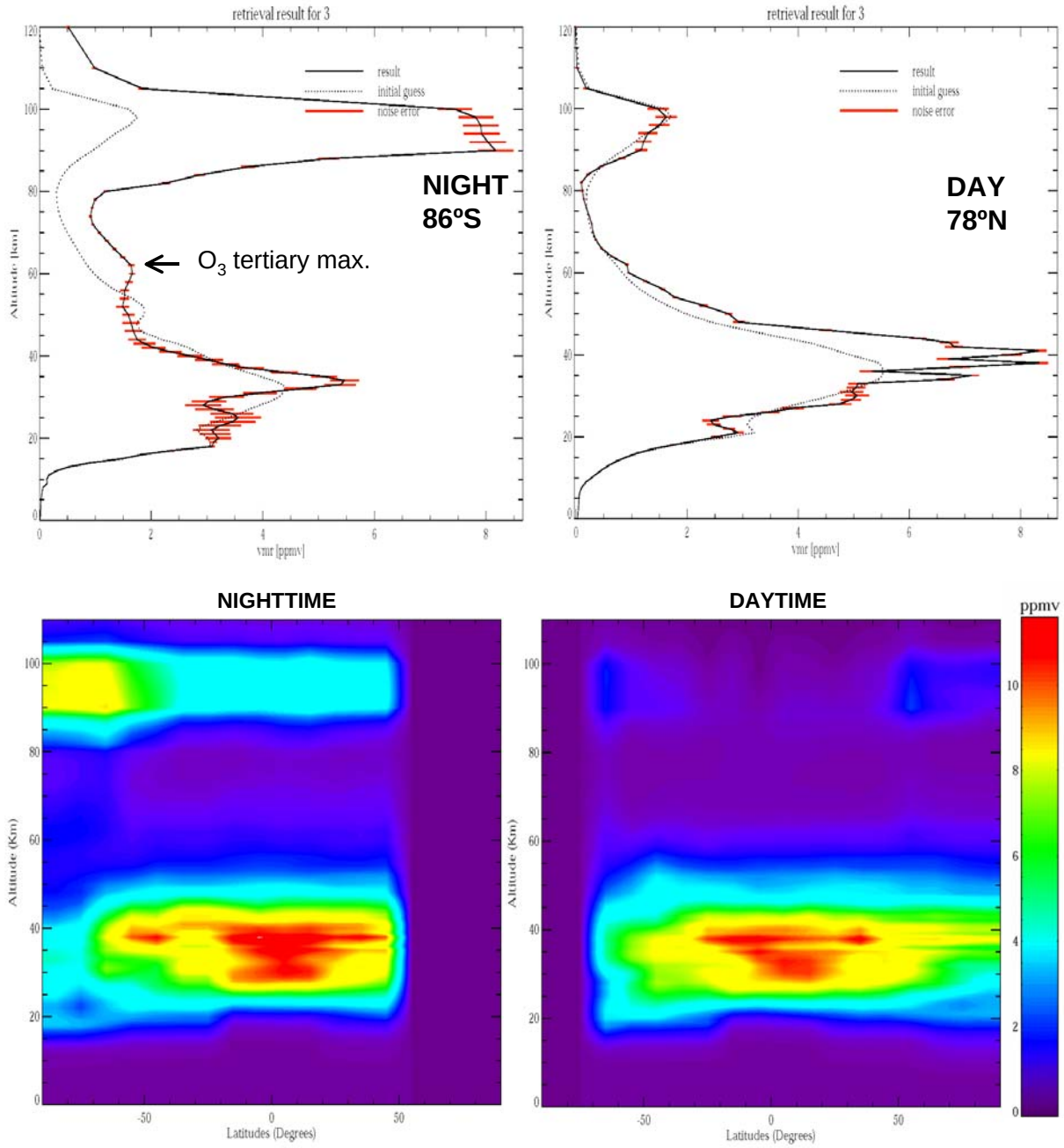

Fig. WP6-1-4: Zonal mean distribution averaged over 4 orbits on 1 July 2002 for night (left) and day (right). Individual profiles are also shown as examples. During night time, the secondary ozone maximum at 95 km and the tertiary ozone maximum at about 60 km over the winter pole are clearly present.

Fig. WP6-1-5 shows the derived temperature field along orbit #6694 (measured on 11 June 2003) while in Fig. WP6-1-4 the ozone field averaged over data from 4 orbits measured on 1 July 2002 is shown. In Fig. WP6-1-5, the sunlit observations are in the left part of the orbit. The retrieval scheme for the temperature produces reliable results for altitudes between ca. 20 and 90 km. Above 80 km the vertical resolution is rather low (> 15 km) due to the large scanning step widths. For the ozone distribution, the secondary ozone maximum near 95 km altitude in the night-time part of the orbit and even the tertiary ozone maximum over the South pole around 60 km altitude are clearly visible.

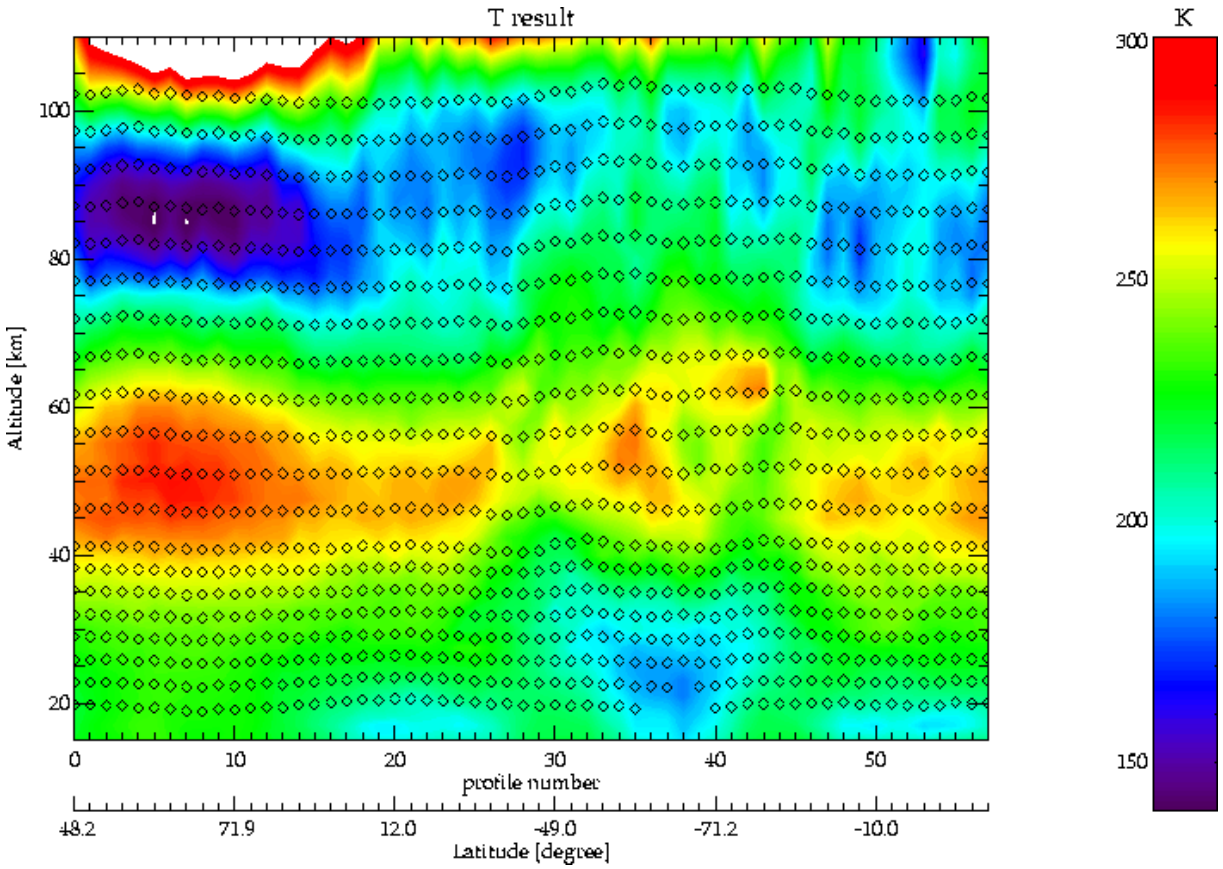

Fig. WP6-1-5: Temperature distribution along orbit # 6694 measured on June 11, 2003. The very low temperatures in the polar summer mesopause are clearly visible; the vertical resolution above 80 km altitudes, however, is only about 15 km.

Validation

MIPAS temperatures retrieved on LTE basis according to (Clarmann et al., 2003b) were compared to HALOE and SABER satellite data (Wang et al., 2004a, 2004b) and LIDAR temperature measurements. There seems to be a small negative bias in MIPAS data in the stratopause region of about -0.7 K (compared to HALOE). The comparison to LIDAR data is inconclusive since it depends strongly on the profiles selected for comparison (see Fig. WP6-1-6).

The comparison of upper stratospheric/mesospheric ozone profiles to GOMOS data (Verronen et al., 2004) is very promising. The secondary and tertiary maxima are found at the same altitudes. Above 90 km, however, differences of up to 2 ppmv occur for night time observations.

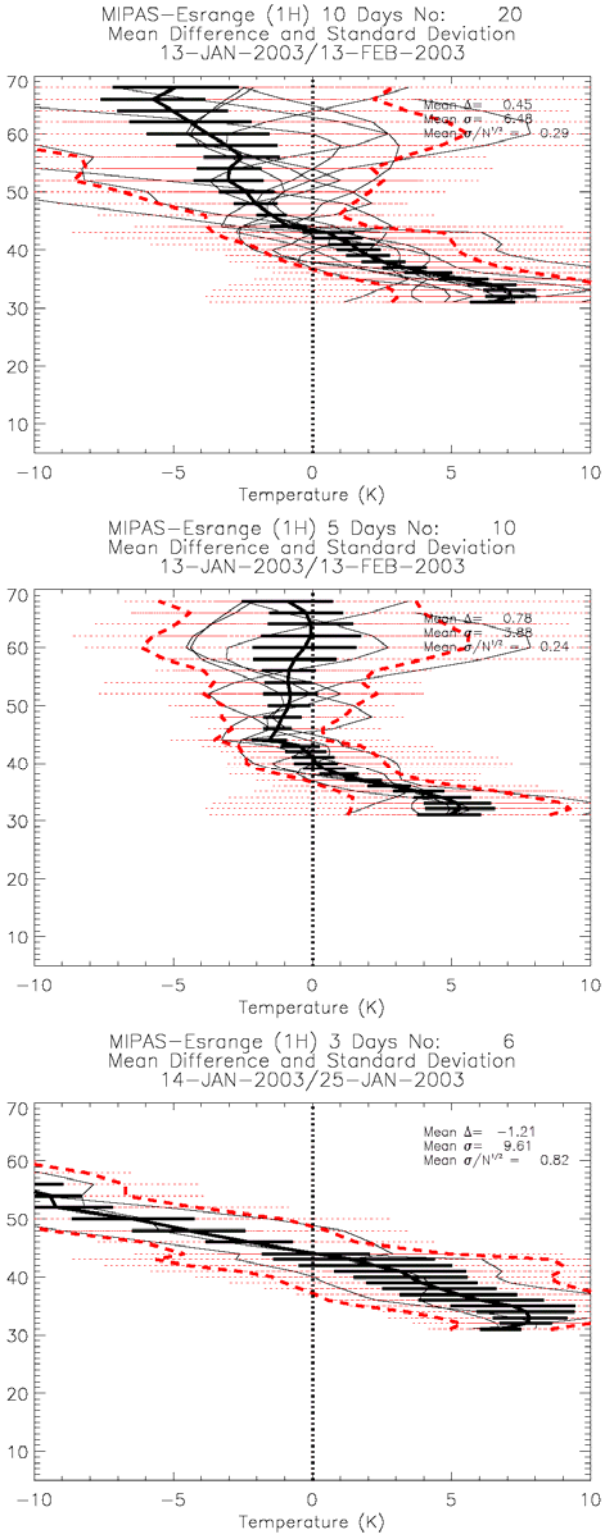

Fig. WP6-1-6: Comparison between the IMK and Esrange LIDAR temperatures. Shown are the averages over 3 (bottom), 5 (middle), and 10 (top) days. The 3 days are 14, 23, and 25 January 2003. The 5 days are 13 and 22 January, and 7, 10, and 13 February 2003. The 10 days are the 3 and 5 days, plus 27 January and 5 February 2003. The adjustment of vertical resolution and *a priori* iof MIPAS s applied to the LIDAR profiles. (LIDAR data courtesy K.H. Fricke, Universität Bonn).

Measurements of temperature, NO_x, CO and ozone in the middle atmosphere by MIPAS/ENVISAT

Although still in the commissioning phase ESA released MIPAS/ENVISAT data for scientific use covering the period of the Antarctic major warming in September/October 2002. At IMK/University of Karlsruhe global data sets on the distribution of a number of trace species were retrieved for the observation days 24 July, 18 to 27 September, and 11 to 13 October 2002, among those in particular CO, NO, and NO_2 (see Fig. WP6-1-7).

In the context of the Antarctic vortex split episode it could be demonstrated by correlations between CO and NO_x (= $NO+NO_2$) that during the polar night (24 July 2002) high volume mixing ratios of NO_x is transported downwards from the upper atmosphere into the stratosphere (see Figs. WP6-1-7 and WP6-1-8). Under equinox conditions, however, NO_x poor air masses are transported downwards (see Fig. WP6-1-8). From this we conclude that in September MIPAS observed the NO_x transport barrier which is formed by the sunlit mesosphere due to the photolysis taking place there (Funke et al., 2003, 2004).

At the end of the reporting period we started to analyse the measurements of the episode of the solar storm in October/November 2003. First results on the temporal evolution averaged over the polar caps for the period 21 October to 12 November 2003 on NO_x and O_3 are given in Fig. WP6-1-9.

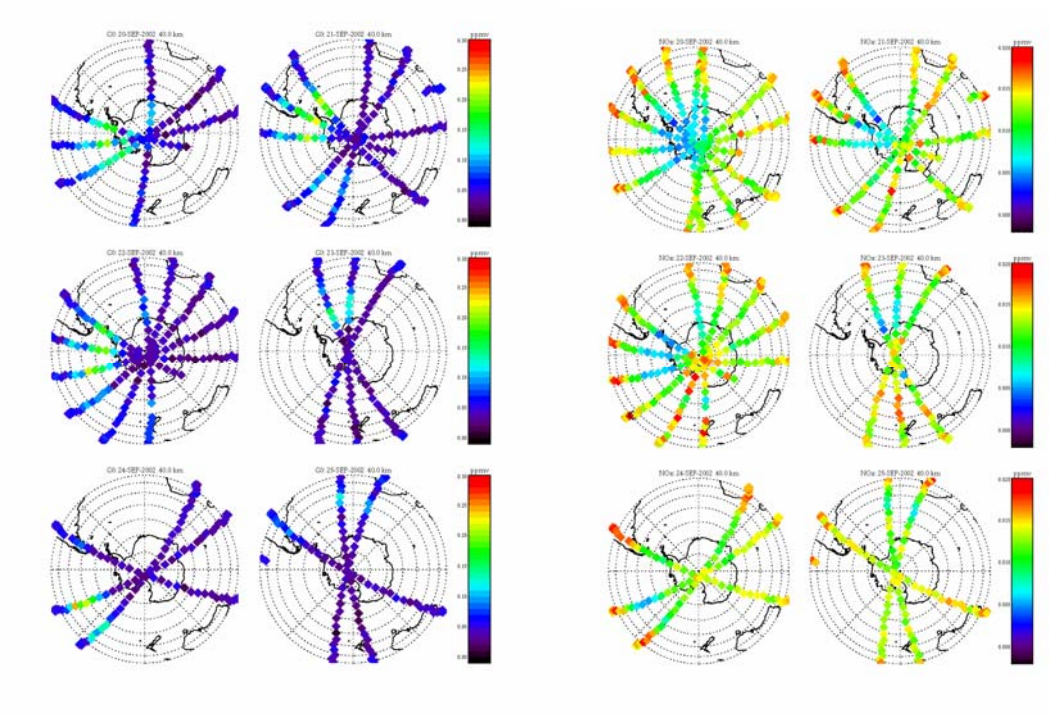

Fig. WP6-1-7: Distribution of CO (left panel) and NO_x (right panel) on the 40 km altitude surface along the MIPAS orbits for the observation days between 20 and 25 September 2002. High CO vmrs are correlated with low NO_x vmr which shows the downward transport of NO_x poor air from the upper atmosphere into the stratosphere.

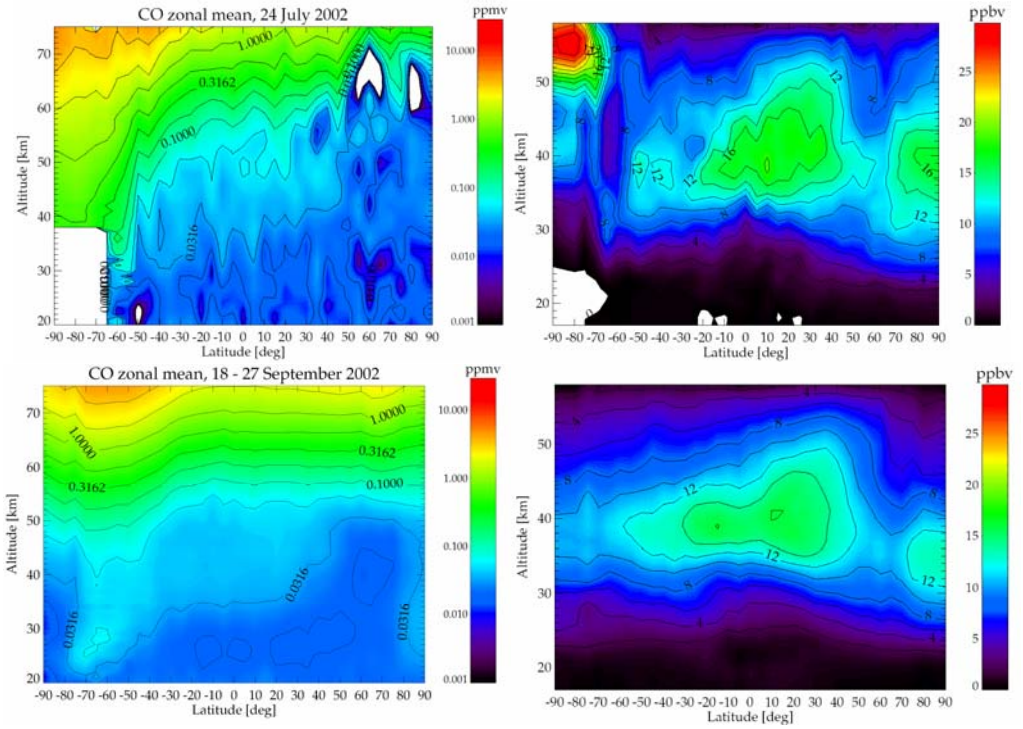

Fig. WP6-1-8: Zonal mean distributions of CO (left column) and NO_x (= NO+NO2) (right column) from MIPAS measurements on 24 July 2002 (upper row) and 18-27 September (lower row). While for both periods, strong downward transport of mesospheric air inside the Antarctic polar vortex is observed from the CO distributions, only during polar night high NO_x concentrations are transported from the thermosphere into the upper stratosphere.

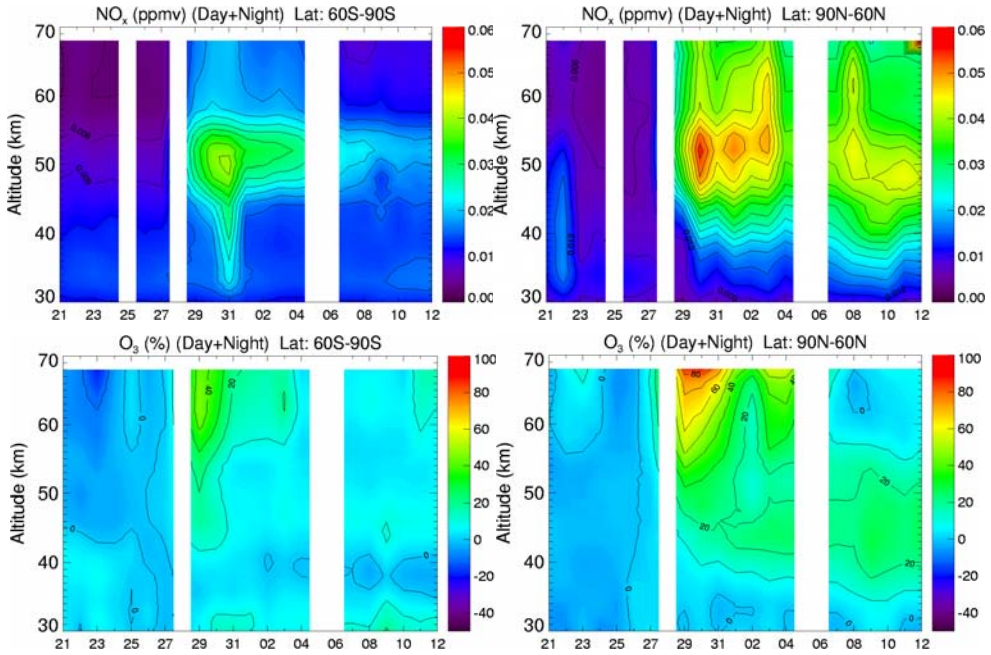

Fig. WP6-1-9: Temporal evolution of NO_x (upper row) and O_3 (lower row) mean values for the Northern (right) and Southern (left) polar cap (60º-90º N/S) between 21 October and 12 November 2003. NO_x is shown in absolute values (ppmv), while for O_3 the percent change relative to the mean value on 27 October 2003 is shown. For NO_x extremely high mean values of up to 60 ppbv occur after the first solar proton events on 28 October. O_3 changes by up to -80 % in the mesosphere on 29 October and 4 November, but recovers rapidly. The stratospheric change is up to -20 % and persistent over the observation time.

NO_x shows an enormous increase (up to 65 ppbv, background values are ~10ppbv), particularly in the NH (winter pole). The change is larger at poleward latitudes, reaching values larger than 100 ppbv at the 80N-90N cap and individual scans up to 130 ppbv. Note the correlation with solar proton events (SPEs) on 28, 29 October and 3 November but shifted by ~1 day. The first SPE on 26 October was weak and no change is observed in NO_x. An increase is also seen around 9-10 November. The reason for this is not clear (weak SPE?, downward transport?). The change in the Southern cap (summer pole) is seen only for the two major SPEs on 28 and 29 October and it decreases rather quickly, restoring to near background levels in about one week. The role of the meridional circulation together with the illumination conditions are the key points for explaining the polar asymmetry. It should be noted that the local initial production (peaks on 29-31 October) are similar in both hemispheres. The NO_x produced in the polar winter is transported downward by the meridional circulation. The dark conditions in NH (<80ºN) together with the downwards transport (injecting NO_x into the stratosphere where NO cannot be destroyed by sunlight) make NO_x concentrations to be larger and more persistent. The lower edge of NO_x, e.g., the 20-ppbv contour, is getting lower as time passes by. On the other hand, in the SH polar summer, the upwelling transport and the longer illumination rapidly destroy NO_x, through NO photolysis at altitudes above ~50 km (López-Puertas et al., 2004).

O_3 depletion caused by both enhanced HO_x and NO_x are evident. The first appears at higher altitudes (blue regions) and have a short life (hours to days). The second, due to the increase in NO_x, is larger, longer and deeper. The good correlation between O_3 depletion and NO_x in the NH polar cap, the shape of the decrease, the downwards shift of the lower edge should be noted. Even the NO_x increase around 9-10 November at ~45 km seems to be also reflected in a corresponding O_3 decrease. O_3 is reduced between 20-100%, depending on the time and altitude. The reduction, as for NO_x, is also larger towards the poles. In the SH polar cap the decrease is smaller and seems to be associated with the short-lived HO_x production only. The O_3 depletion by NO_x seems to be rather weak in this hemisphere (López-Puertas et al., 2004).

References

B. Funke, M. López-Puertas, G. Stiller, T. v. Clarmann, M. Höpfner, and M. Kuntz, Non-LTE State Distribution of Nitric Oxide and its Impact on the Retrieval of the Stratospheric Daytime NO Profile from MIPAS Limb Sounding Instruments, Adv. Space Res., 26, 947-950 (2000)

B. Funke, M. López-Puertas, G.P. Stiller, T. von Clarmann, and M. Höpfner, A New NLTE Retrieval Method for Atmospheric Parameters From MIPAS-ENVISAT Emission Spectra, Adv. Space Res., 27, 1099-1104 (2001)

B. Funke, M. López-Puertas, F.J. Martín-Torres, G. Stiller, and T. von Clarmann, A New Non-LTE Retrieval method for Atmospheric Parameters from MIPAS-ENVISAT Emission Spectra, in: Schäfer, K., Lado-Bordowsky, O., Comeron, A., Carleer, M.R., Fender, J.S. (Eds.), Remote Sensing of Clouds and the Atmosphere VI, Proceedings of SPIE, Vol. 4539, 396-405 (2002)

B. Funke, T. von Clarmann, H. Fischer, M. García-Comas, S. Gil-López, N. Glatthor, U. Grabowski, M. Höpfner, S. Kellmann, M. Kiefer, A. Linden, M. López-Puertas, M.Á. López-Valverde, G. Mengistu Tsidu, M. Milz, T. Steck, G. P. Stiller, and D.-Y. Wang , Non-LTE retrieval of NO, NO2, and CO from MIPAS-ENVISAT, 11th International Workshop on Atmospheric Science from Space Using Fourier Transform Spectrometry (ASSFTS), Bad Wildbad, 8-10 October 2003, Germany, (2003)

B. Funke, M. López-Puertas, T. von Clarmann, G.P. Stiller, H. Fischer, N. Glatthor, U. Grabowski, M. Höpfner, S. Kellmann, M. Kiefer, A. Linden, G. Mengistu Tsidu, M. Milz, T. Steck, and D.-Y. Wang, Retrieval of stratospheric NO_x from 5.3 and 6.2 mum non-LTE emissions measured by MIPAS on ENVISAT, J. Geophys. Res., submitted July 2004 (2004)

S. Gil-López and the IMK-IAA MIPAS/ENVISAT Team, Stratospheric and Mesospheric Ozone Derived from MIPAS/ENVISAT under Consideration of non-LTE, EGS-AGU-EUG Joint Assembly in Nice, France from 06-11 April 2003, (2003)

M. López-Puertas, F.J. Martín-Torres, B. Funke, M.A. López-Valverde, T. von Clarmann, G. Stiller, H. Oelhaf, H. Fischer, J.M. Flaud, Non-LTE Studies for the analysis of MIPAS/Envisat data, in:

Schäfer, K., Lado-Bordowsky, O., Comeron, A., Carleer, M.R., Fender, J.S. (Eds.), Remote Sensing of Clouds and the Atmosphere VI, Proceedings of SPIE, Vol. 4539, 381-395 (2002a)

M. López-Puertas, T. von Clarmann, A. Dudhia, J.-M. Flaud, B. Funke, M. García-Comas, S. Gil-López, N. Glatthor, U. Grabowski, V. Jay, M. Kiefer, M. López-Valverde, Gaetan Perron, G. Stiller, Analysis of Non-LTE Effects in the MIPAS/ENVISAT Data, in: H. Sawaya-Lacoste (Ed.), ENVISAT Calibration Review - Proceedings of the European Workshop, 9 - 13 September 2002, ESTEC, Noordwijk, The Netherlands, ESA SP-520, CD-ROM (2002b)

M. López-Puertas, T. von Clarmann, A. Dudhia, J.-M. Flaud, B. Funke, M. García-Comas, S. Gil-López, N. Glatthor, U. Grabowski, V. Jay, M. Kiefer, M.A. Lopez-Valverde, G. Perron, and G. Stiller, Non-LTE studies for the validation of MIPAS L2 products, Proc. Envisat Calibration Review, ESA SP-531, http://envisat.esa.int/pub/ESA_DOC/envisat_val_1202/proceedings/, (2003a).

M. López-Puertas, T. von Clarmann, H. Fischer, B. Funke, M. García-Comas, S. Gil-López, N. Glatthor, U. Grabowski, M. Höpfner, S. Kellmann, M. Kiefer, A. Linden, M. Á. López-Valverde, G. Mengistu Tsidu, M. Milz, H. Oelhaf, T. Steck, G. P. Stiller, and D.-Y. Wang , The temperature and CO2 abundance of the mesosphere and lower thermosphere as measured by MIPAS/ENVISAT, 11th International Workshop on Atmospheric Science from Space Using Fourier Transform Spectrometry (ASSFTS), Bad Wildbad, 8-10 October 2003, Germany (2003b)

M. López-Puertas, B. Funke, T. von Clarmann, H. Fischer, S. Gil-López, N. Glatthor, U. Grabowski, M. Höpfner, M. Kaufmann, S. Kellmann, M. Kiefer, M.E. Koukouli, A. Linden, G. Mengistu Tsidu, M. Milz, T. Steck, G.P. Stiller, and D.-Y. Wang, Atmospheric Effects due to the October-November 2003 Solar Proton Events as Observed by MIPAS/ENVISAT, COSPAR 2004, 18-25 July 2004, Paris, France, (2004)

G.P. Stiller, T. von Clarmann, T. Chidiezie Chineke, H. Fischer, B. Funke, S. Gil-López, N. Glatthor, U. Grabowski, M. Höpfner, S. Kellmann, M. Kiefer, A. Linden, M. López-Puertas, G. Mengistu Tsidu, M. Milz, and T. Steck, Early IMK MIPAS/ENVISAT results, in: K. Schäfer, O. Lado Bordowsky (Eds.), Remote Sensing of Clouds and the Atmosphere VII, Proceedings of SPIE, Vol. 4882, pp. 184 - 193 (2003)

G.P. Stiller, T. v. Clarmann, B. Funke, N. Glatthor, F. Hase, M. Höpfner, and A. Linden, Sensitivity of trace gas abundances retrievals from infrared limb emission spectra to simplifying approximations in radiative transfer modeling, JQSRT, 72, 249-280 (2002)

P.T. Verronen, E. Kyrölä, B. Funke, S. Gil-López, M. Kaufmann, M. López-Puertas, T. von Clarmann, G. Stiller, U. Grabowski, and M. Höpfner, A Comparison of night-time GOMOS and MIPAS vertical ozone profiles, Adv. Space Research, in preparation (2004).

T. von Clarmann, T. Chidiezie Chineke, H. Fischer, B. Funke, S. Gil-López, N. Glatthor, U. Grabowski, M. Höpfner, S. Kellmann, M. Kiefer, A. Linden, M. López-Puertas, G. Mengistu Tsidu, M. Milz, T. Steck, and G.P. Stiller, Remote sensing of the middle atmopshere with MIPAS, in: K. Schaefer, O. Lado Bordowsky (Eds.), Remote Sensing of Clouds and the Atmosphere VII, Proceedings of SPIE, Vol. 4882, pp. 172 - 183 (2003a)

T. von Clarmann, N. Glatthor, U. Grabowski, M. Höpfner, S. Kellmann, M. Kiefer, A. Linden, G. Mengistu Tsidu, M. Milz, T. Steck, G.P. Stiller, D.Y. Wang, H. Fischer, B. Funke, S. Gil-López, M. López-Puertas, Retrieval of temperature and tangent altitude pointing from limb emission spectra recorded from space by the Michelson Interferometer for Passive Atmospheric Sounding (MIPAS), J. Geophys. Res., 108, doi: 10.1029/2003JD-003602 (2003b).

D.-Y. Wang, G. Stiller, T. von Clarmann, M. García-Comas, M. López-Puertas, M. Kiefer, M. Höpfner, N.Glatthor, B. Funke, S. Gil-López, U. Grabowski, S. Kellmann, A. Linden, G. Mengistu Tsidu, M. Milz, T. Steck, H. Fischer, J. Russell III, E. E. Remsberg, C. J. Mertens, and M. G. Mlynczak, Comparisons of MIPAS-observed temperature profiles with other satellite measurements, Remote Sensing of Clouds and the Atmosphere VIII, K. P. Schäfer, A. Comerón, M. Carleer, R.H. Picard (eds.), Proc. of SPIE, Vol. 5235 (SPIE, Bellingham, WA, 2004), 196-207 (2004a).

D.-Y. Wang et al., Validation of stratospheric temperatures measured by MIPAS on ENVISAT, to be submitted to J. Geophys. Res., in prepration (2004b).

Contribution of IMK-KASIMA

Solar variability: CTM-studies of photolysis

The influence of solar variability on the state of the atmosphere is well documented in climatic records but still the principal mechanism seems not to be understood. Concentrating on radiative effects, one major obstacle when modelling solar influence is the sophisticated spectral variability of the solar radiation, it's coupling to stratospheric chemistry and the subsequent interaction with dynamics. Therefore a detailed examination of photolysis codes and UV radiation transfer is a prerequisite when modelling the influence of solar variability on the state of the atmosphere. The work within KODYACS concentrated on studies of radiation transfer for photo chemically important wavelengths with a high solar variability, the comparison of photolysis codes and their results for variable solar input. Within the project, a hitherto overseen effect by atmospheric refraction was found which may be important for downward transport of solar activated air masses in polar night situation.

Penetration of Lyman-α radiation

The solar variability has a strong spectral dependence, with the maximum variation in the UV and EUV part of the solar spectrum. Most of this radiation cannot penetrate the mesosphere and the uppermost stratosphere through the strong absorption by molecular oxygen. By chance, the highly variable and UV dominant solar Lyman-α line coincides with a deep minimum of the O_2 absorption cross section, thereby giving Lyman-α photons a dominating role for photolysing CH_4, CO_2, and H_2O in the mesosphere. Within most models of the middle atmosphere the Lyman-α flux is parameterised by a simple exponential. Chabrillat and Kockarts (1997) showed that these parameterisations are not sufficient to describe the Lyman-α flux in the mesosphere as the O_2 absorption cross section has a temperature dependence which in addition varies over the spectrally resolved solar Lyman-α line profile. They give an improved parameterisation based on a sum of exponentials of the O_2 slant column. In fact, their scheme does not include a detailed treatment of solar zenith angle dependence and the dependence of seasonal changes of the temperature profile within the mesosphere. In addition, determination of the Lyman-α photon density (which is equivalent to actinic flux) is further complicated by Lyman-α resonant scattering in the terrestrial atmosphere giving rise to a prominent diffuse Lyman-α field, and also influenced by the variation of the form of the solar Lyman-α line profile during phases of enhanced solar activity. Both effects are not included in parameterisations used in models of the middle atmosphere. As for the chemically relevant altitude range the optical depth for Lyman-α is significant, even small changes in the outer conditions may produce observable effects in the photolysis rates.

The evaluation of these combined effects demands a detailed wavelength dependent description of scattering and absorption processes of Lyman-α photons within the atmosphere. For that purpose a Monte Carlo program (MCP) was developed which takes into account the temperature dependent absorption by molecular oxygen and multiple resonance scattering by atomic hydrogen within the terrestrial atmosphere. Resonant scattering is treated with partial frequency redistribution caused by the associated Doppler effect but the natural line-width is neglected. As we are mainly interested in the mesosphere, a plane parallel atmosphere is assumed, but to include resonant scattered photons in the exosphere the outer boundary for the model is set at 1000 km. For each parallel stratum the temperature and the densities of O_2 and H are taken from the MSIS-90 model or as a combination of standard profiles and model output from the KASIMA model. Results of the calculations of the spectrally resolved Lyman-α region at different altitudes are shown in Fig. WP6-2-1.

Whereas for the determination of the dissociation rates of H_2O, CH_4 and other species the integrated photon density is sufficient, the O_2 dissociation rate is determined within the model as the integration over the Lyman-α spectrum. In addition, Lacoursiere et al. (1999) showed that the O(1D) yield of Lyman-α

absorption is wavelength dependent, too, within the interval of the line width of the Lyman-α line. The determination of this yield is also included in the MCP module (see Fig. WP6-2-3).

For the estimation of the combined effects, typical T-, O_2- and H-profiles taken from the MSIS model for equinox and solstice conditions for different solar zenith angles have been used and compared with the Chabrillat and Kockarts parameterisation.

Generally, the results obtained show that for an overhead sun the parameterisation given by Chabrillat and Kockarts yields a good agreement with the exact results of the MCP at altitudes below 100 km (see Fig. WP6-2-2). Above 100 km altitude, the resonant scattering increases the photon density in the centre of the line up to factor 2. The O(1D) yield is found to decrease from about 58% for an undisturbed Ly-α line profile to about 48% at 60 km altitude. For slant optical paths, the situation is different. Here even without including the effects of resonant scattering differences exceeding 10% are found at 70 km altitude. Regarding the effect of resonant scattering, Figure WP6-2-1 shows as an example the atmospheric Ly-α line profile for Dec 21, 1200 UT, at 60° N at different altitudes below 100 km. Here, Ly-α photons found below 75 km have predominantly been scattered in the atmosphere. Both effects seem to increase Lyman-α photon density, but one should note that this occurs generally at large τ.

To account for different temperature profiles and in order to include the contribution of scattered photons a parameterisation of the form $Q = f \exp(-\tau) + Qs$ was proposed where the parameter τ is given as a polynomial of two representative temperatures and the O_2 column. Up to a column density of O_2 of about 10^{25} m^{-2} the deviations between exact and approximate solution are less than 5%. For small O_2 columns the effect of resonance scattering is less than about 5%, whereas the influence of different temperature profiles exceeds 5% above $2x10^{24}$ m^{-2} for cases where the temperature deviates from standard conditions, see Fig. WP6-2-2. Further tests show that the parameterisation gives results within 20% compared with the MCP results for attenuations up to 10^{-6} for the cases studied. In addition, parameterisations have been prepared for O_2 photolysis rate and the O(1D) yield. Details can be found in Reddmann and Uhl (2002).

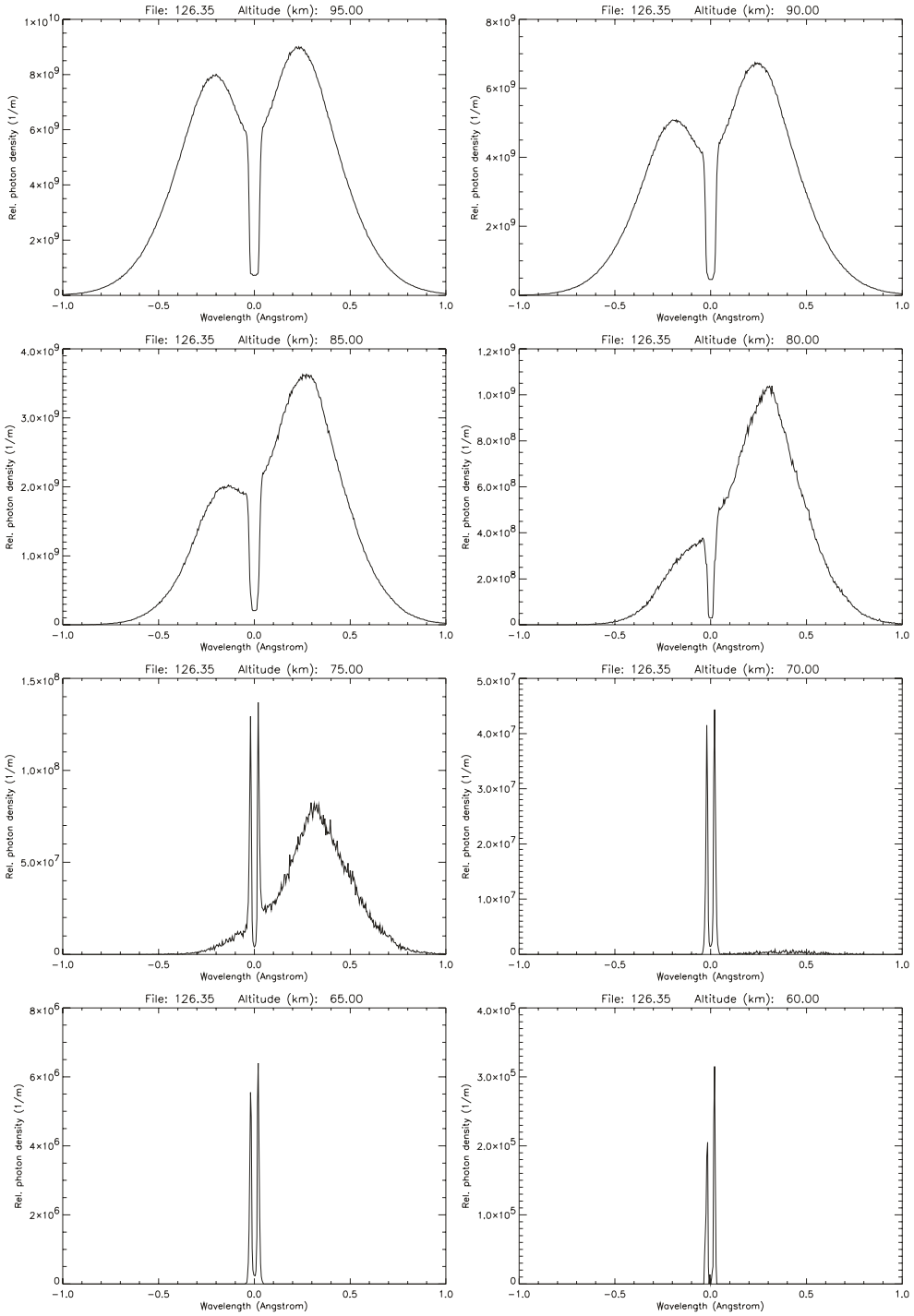

Fig. WP6-2-1: Terrestrial spectrum of the solar Lyman-α line at different altitudes for Dec-21, 1200 UT at 60°N.

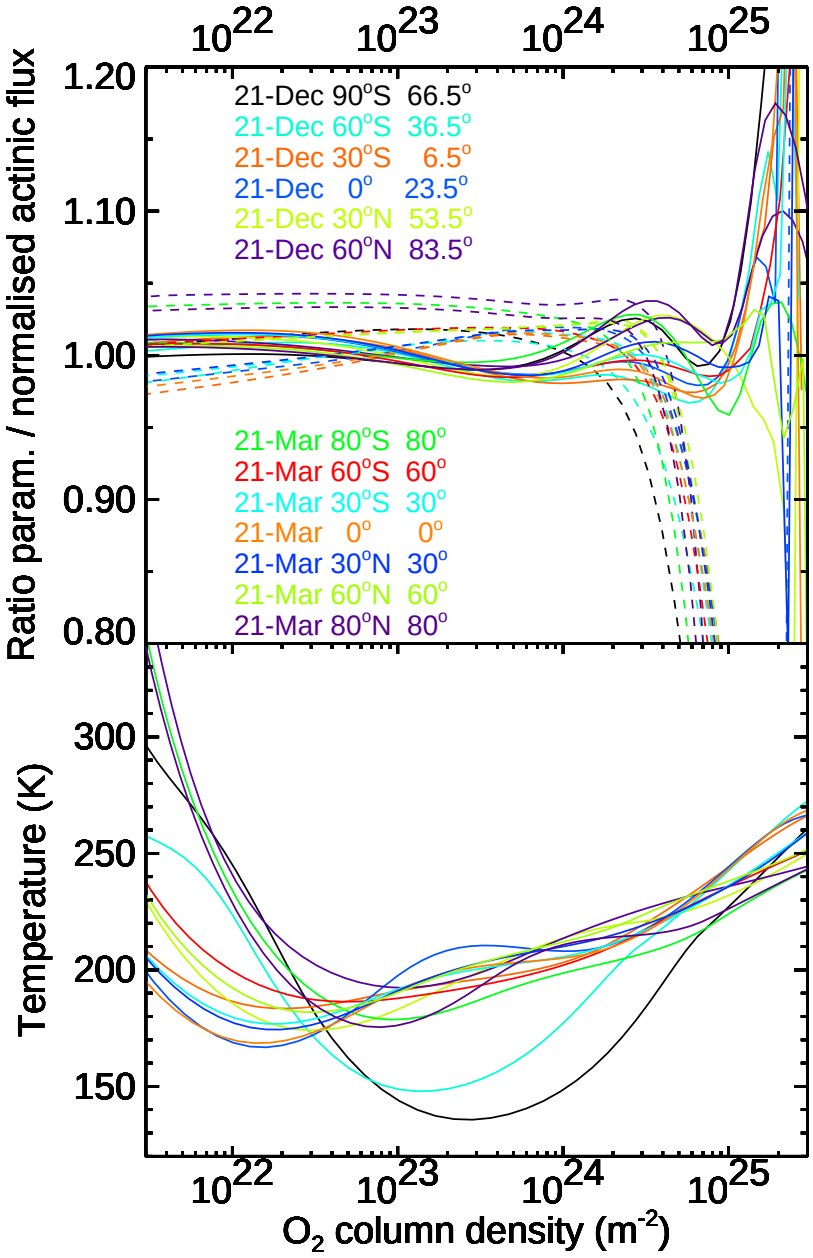

Fig. WP6-2-2: Comparison of the parameterization by Chabrillat and Kockarts (dashed line) and the MCP based results given as a ratio to the exact MCP results Top) for different temperature profiles (bottom).

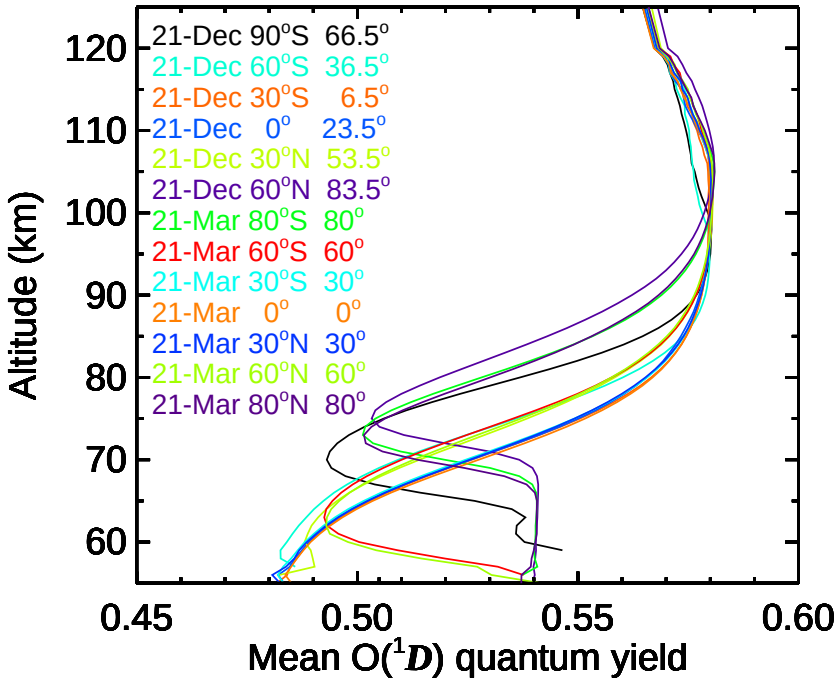

Fig. WP6-2-3: Variation of O(1D)-quantum yield for the solar Lyman-α line with height for different temperature profiles (see Fig. WP6-3)

Photolysis

Comparison of different photolysis modules in cooperation with the TOPOZ III EU project showed significant deviations in the UV spectral region near 200 nm (Ruhnke et al. 2002) (see Fig. WP6-2-4). This spectral region is also important in terms of solar variability effects as below the Al-edge at 205 nm the solar cycle variation is about 10% compared to about 5% below 300 nm, and solar radiation can deeply penetrate into the atmosphere between the Schuman-Runge absorption bands. In addition, scattered radiation at 200 nm is normally not included in photolysis codes, which may be important for high solar zenith angles. To validate the different codes, a new Monte Carlo program was developed to model actinic flux with spherical geometry and to include Rayleigh scattering. The results obtained show surprisingly strong deviations at short wavelengths (190 nm) at all zenith angles, and for longer wavelengths (200 nm) strong deviations were found at high solar zenith angles compared to the codes used in different models.

At about 200 nm a very good agreement was found with the fast-j radiation code of M. Prather (priv. communication) up to about 93 deg solar zenith angle (see Fig. WP6-2-6). The on-line fast-j2 had been adapted to the KASIMA model environment.

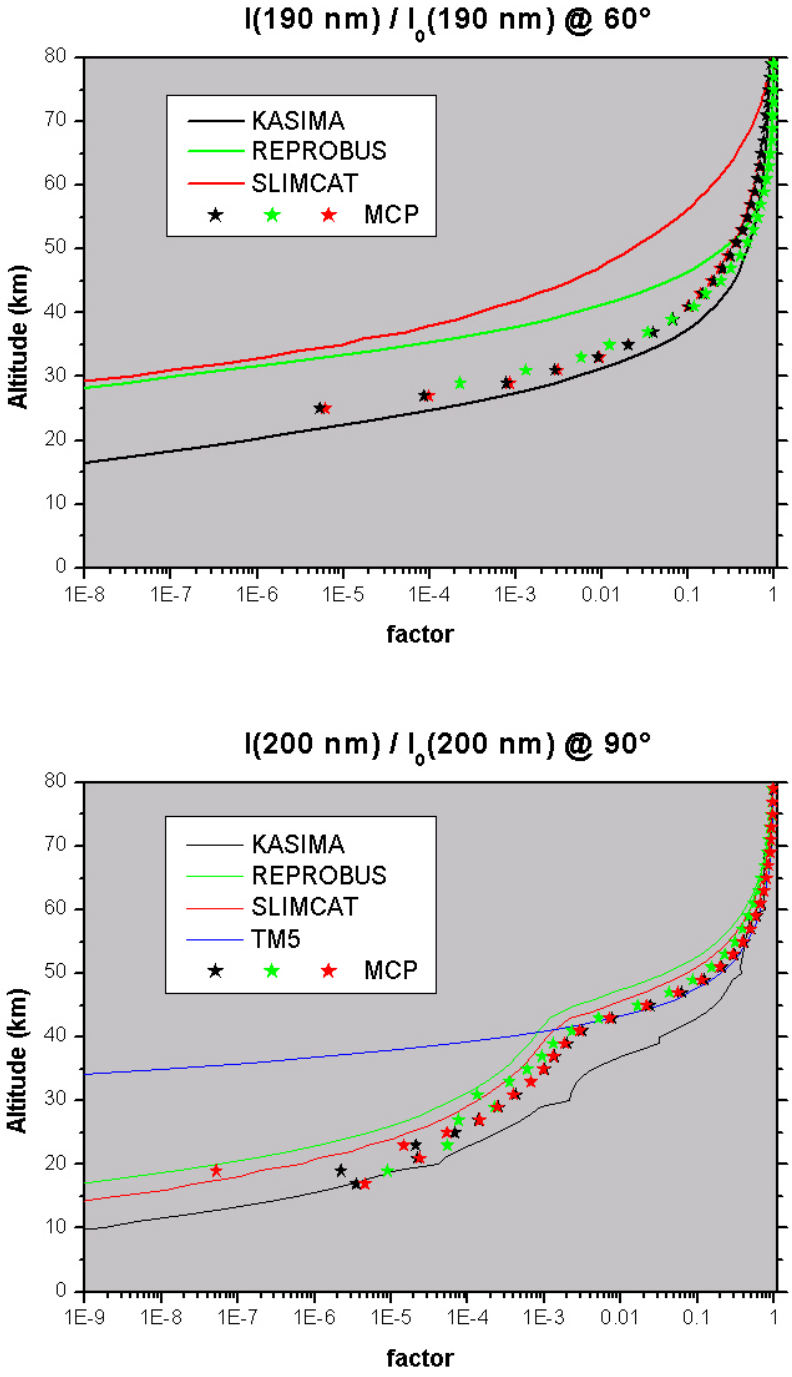

Fig. WP6-2-4: Comparison between parameterization used in different 3D-models and the MCP calculations for two wavelengths. The colour coding of the MCP results corresponds to the specific wavelength intervals of the corresponding parameterizations. For reduction factors smaller than 10e-5, statistical effects of the MC calculations can be noted.

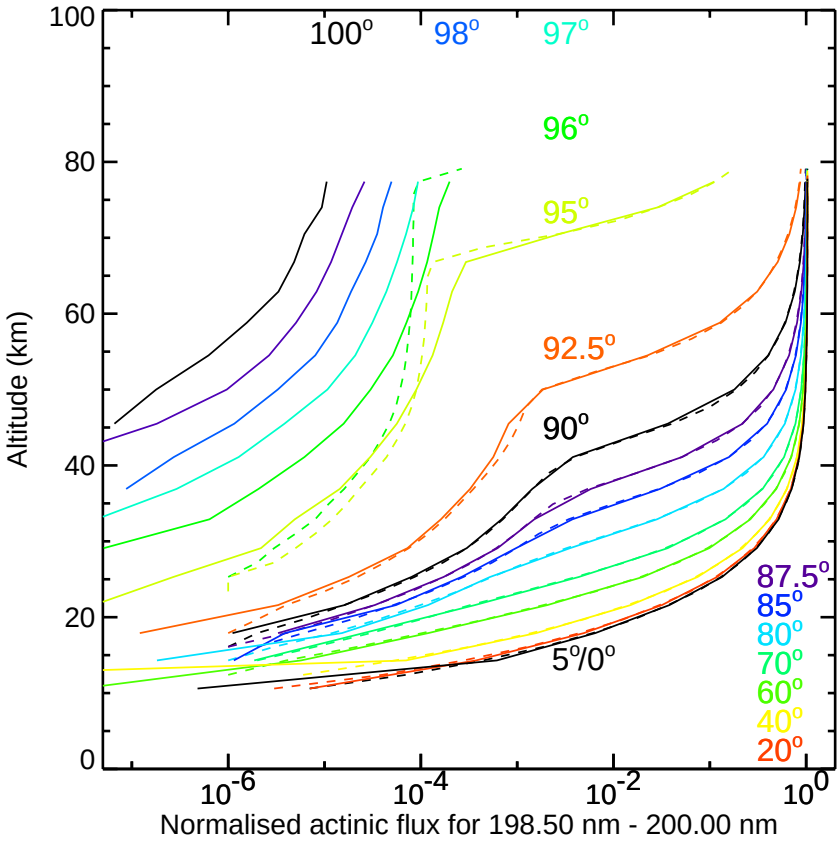

Fig. WP6-2-5: Example of detailed Monte Carlo calculations in the UV spectral region. Dashed lines are the results of the fast-j parameterisation.

In addition, the photolysis code ART used in KASIMA was modified to include the results of our detailed calculations for the UV-part for wavelengths less 200 nm. Fig WP6-2-6 shows the effect on photolysis rates with and without the MCP results. Sensitivity tests using the scheme of Landgraf and Crutzen (plane parallel version) and the ART scheme in KASIMA exhibit significant differences in the effect of solar variability. This again shows that for solar studies photolysis parameterizations with a very good representation of the UV part of the solar spectrum are important.

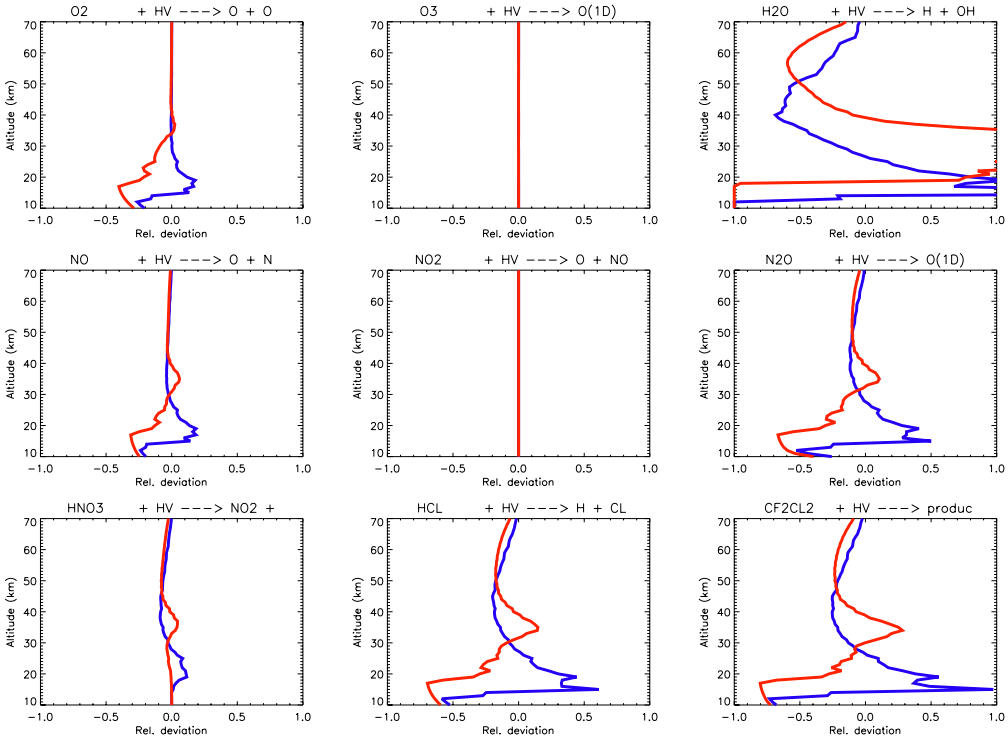

Fig. WP6-2-6: Comparison of photolysis rates when replacing the ART parameterizations by MCP results for wavelengths < 200 nm.

Effects of refraction

Especially for studies related to downward transport of solar produced NOx during polar night, photolysis rates in twilight conditions must be known very well. Some studies show significant effects on the chemical state of the atmosphere near the terminator when refraction is included in photochemical calculations. We found that there is another effect caused by refraction which has been overlooked in previous studies. In addition to an altered optical path with a lower optical depth and hence higher solar flux, refraction causes a divergence of solar rays which reduces the actinic flux (see Fig. WP6-2-7).

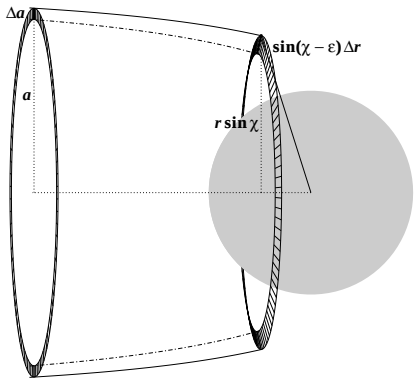

Fig. WP6-2-7: Scheme showing the divergence effect caused by refraction: the higher bending of solar rays in deeper layers causes solar rays to diverge, and thus the actinic flux is reduced.

Our calculations of this effects and the combination of altered optical pathway show, that by the compensation of refraction effects related to a changed optical path through the divergence effect the region around the terminator where refraction considerably affects actinic flux is narrowed. Therefore it may probably be justified to neglect refraction in photochemical calculations, at least for background aerosol conditions. Fig. WP6-2-8 shows the change of transmittance, the divergence effect and their combination near the terminator for a specific meteorological condition.

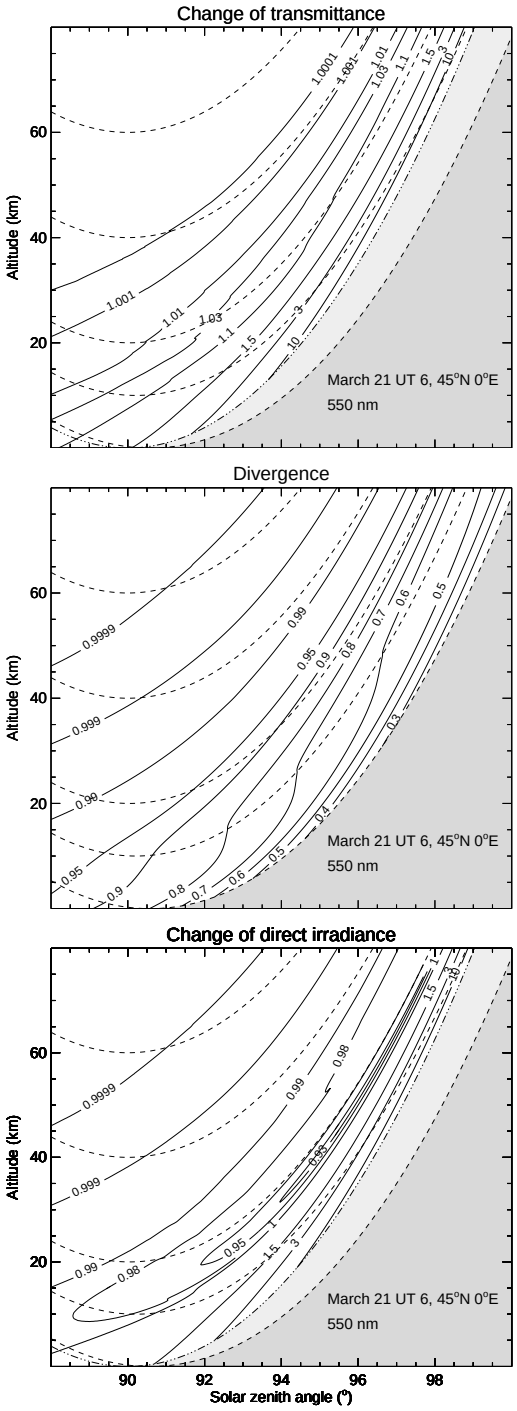

Fig. WP6-2-8: Effects of refraction on direct solar irradiation. Top: effects by changed optical path alone, mid: by divergence alone, bottom: combination of both effects.

New publications with contributions from WP6

Reddmann, T. and Uhl, R., The H Lyman- actinic flux in the middle atmosphere Atmospheric Chemistry and Physics, Vol. 3, pp 225-231, 20-2-2003

Reddmann, T., Ruhnke, R. and Uhl, R., A detailed Examination of Photolysis Rates in the EUV Geophysical Research Abstracts, Vol. 5, pp -, 30-1-2003

Reddmann, T., Kouker, W. and Ruhnke, .Tracer Studies with the 3-D CTM KASIMA, EGS XXVII General Assembly 2002, Nice, France

Reddmann, T. and Uhl, R., The solar Hydrogen Lyman-a photon density within the mesosphere, EGS XXVII General Assembly 2002, Nice, France

Ruhnke, R., B. Bregman, M. Chipperfield, J. Landgraf, F. Lefèvre, and T. Reddmann, Intercomparison of photolysis rates calculated by 3D CTMs, Proceedings of the 6th European Symposium on Stratospheric Ozone, Göteburg, Sweden, 2002.

Uhl, R., Reddmann, T. and Ruhnke, R. Actinic flux in the EUV at deep atmospheric layers: a Monte Carlo programme, Geophysical Research Abstracts, Vol. 5, pp -, 30-1-2003.

Uhl, R. and Reddmann, T. Divergence of sun-rays by atmospheric refraction at large solar zenith angles, Atmospheric Chemistry and Physics Discussions, Vol. 4, pp 2037-2054, 16-4-2004, accepted for ACP.

Uhl, R. and Reddmann, T. Divergence of sun-rays by atmospheric refraction at large solar zenith angles, EGS XXIX General Assembly 2004, Nice, France

References:

S. Chabrillat and G. Kockarts, Simple parameterization of the absorption of the solar Lyman- line, GRL, 1997, volume=24, pp 2659-2662

J. Lacoursiére, S. A. Meyer, G. W. Faris, T. G. Slanger, B. R. Lewis and S. T. Gibson, The O(1D) yield from O_2 photodissociation near H Lyman- (121.6 nm), JCP, 1999, volume=110, pp 1949-1958

B. R. Lewis, I. M. Vardavas and J. H. Carver, The aeronomic dissociation of water vapor by solar H Lyman- radiation, JGR, 1983, volume=88, pp 4935-4940

Contribution of MPI-MIPS

Influence of volcanoes

Validation of the coupled chemical-microphysical-climate model: a Pinatubo case study

A first version of the CMCM with interactive stratospheric chemistry and prognostic and interactive volcanic aerosol has been employed in a joint action with MPI-C, to analyse the influence of large volcanic eruptions on the stratospheric ozone concentration. Our model results show that the treatment of the volcanic aerosol with a bulk approach and a simple parameterization for the aerosol size distribution can reproduce the observed atmospheric effects after the Pinatubo eruption reasonably well (*Timmreck et al., 2003).*The aerosol mode radius is overestimated in the first months after the eruption which leads to strong perturbations in the heating rates and to enhanced downward transport. The simulated aerosol surface area density corresponds quite well with observations from the Northern Hemisphere midlatitudes (Figure WP6-3-1).

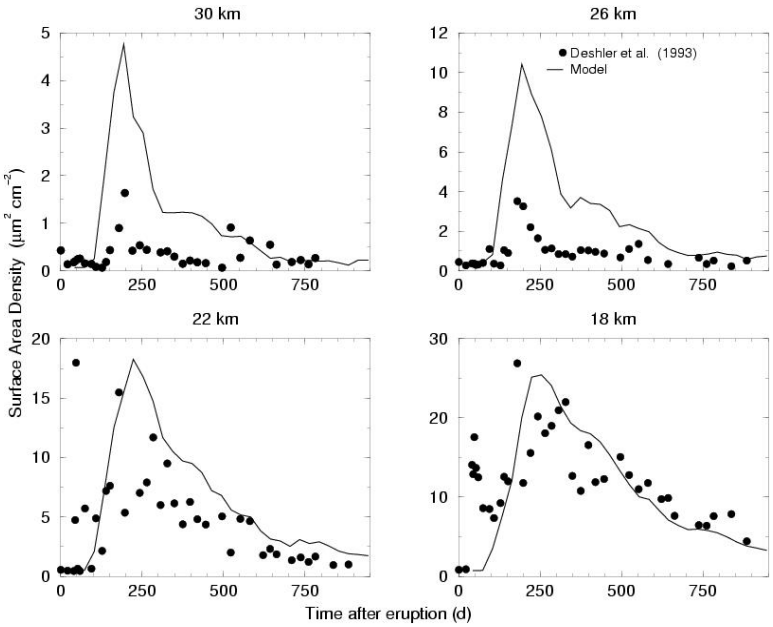

Fig.WP6-3-1: Temporal development of the aerosol surface area density ($\mu m^2 / cm^3$) at 41°N at four altitudes. The circles indicate the measurements (Deshler et al., 1993) and the solid line indicates the simulated monthly mean values for the corresponding grid.

Generally, the temporal development of the aerosol surface area density at Laramie is well represented by the GCM simulations, in particular at 22 km and 18 km. The model however, does not reproduce the first distinct maximum three weeks after the eruption in July. This originates from a smaller eruption plume from June 12th, which injected material at lower altitudes. This eruption plume has not been considered in our simulation. In the two upper layers at 30 km and 26 km the model simulation overestimates the observation by an factor of 2-3. This is related to difficulties in the simulated long range transport and to numerical vertical diffusion in the model.

The simulated changes in the atmospheric trace gas concentration looks reasonable. The changes in the chemical concentration due to the volcanic aerosol are a combined effect of changes in the heterogeneous chemistry, in the photolysis rates and in the heating rates.

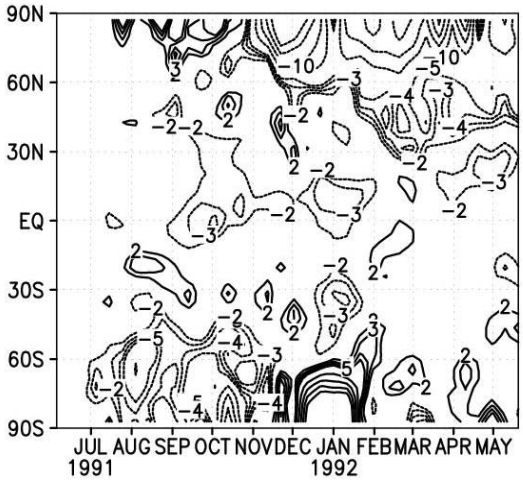

Fig WP6-3-2: Total ozone changes % in the first year after the Pinatubo eruption.

Figure WP6-3-2 depicts the relative changes in total ozone for the first year after the eruption. Column ozone decreases in the tropics in particular in the NH, by about 2%-3% in autumn 1991 from September 1991 on with a maximum loss of 4% in October 1991. This agrees with QBO detrended observations which estimated total ozone depletion of 2-4% in the equatorial regions (e.g. *Zerefos et al., 1994; Randel et al., 1995; Angell, 1997*). Total ozone increases in the SH in polar summer by more than 25%, three times higher than the ground based observations (*Angell, 1997*). In NH polar winter the simulated total ozone decreases of by more than 20%, which is twice as large as satellite observations of 10% (*Randel et al., 1995*) and ground base estimates of 6.1 Γ2.3% (*Angell, 1997*). We have considered here the difference between two model simulations: a volcanically disturbed and an undisturbed one, both of which are influenced by the meteorology of the particular years. The inter-annual variability in the NH high latitudes is very high. Thus, to simulate ozone changes in high latitudes ensemble simulations of at least five independent runs are necessary, or the meridional circulation has to be forced by the assimilation of dynamical fields (wind, temperature). Ensemble simulations of the Pinatubo episode are planned for a statistically significant assessment of the simulated chemical and dynamical changes.

In addition, a comparison of the simulated ozone changes with observations for different stations has been carried out with the DWD (1.8). Together with Ulrike Lohmann (Dalhousie Univ., Canada) and Bernd Kärcher (DLR) we have also performed different sensitivity studies with the ECHAM general circulation model for 2 ½ years after the Mt. Pinatubo eruption (July 1991 to December 1993) to study the possible potential of volcanic emission to alter cirrus cloud properties (*Lohmann et al., 2003*). We have compared homogeneous cirrus formation caused by sedimenting sulfate particles produced in the eruption plume with homogeneous cirrus formation in the undisturbed atmosphere. In the first scenario, the sulfate aerosol mass from the MAECHAM4/CHEM Pinatubo simulation (*Timmreck et al., 2003*) is added to the background aerosol concentration assuming a monomodal aerosol. Here the aerosol concentration increases by up to 3000 cm^{-3} in 1992, which can be regarded as an upper limit more representative for the first months after the eruption. The ice crystal number concentration increases by up to 1 cm^{-3} near the tropical tropopause more than doubling the pre-existing concentration in this region one year after the eruption. In the second, more realistic, scenario the simulated Pinatubo aerosol is added to a bimodal

background size distribution as a separate large particle mode. Here the aerosol number concentration increases by 10-25 cm^{-3}, which can be regarded as a lower bound more representative for 1992. Then the ice crystal number increases at most 50% in the tropics in 1992. Satellite observations (*Wylie et al., 1994*) show an increase in ice water path and cirrus cloud cover starting in 1992 that could be related to either the Mt. Pinatubo eruption or the El Nino event or both but no systematic trend is seen in cloud optical properties or total cloud cover (*Luo et al., 2002*). While there is no trend on cloud microphysical or optical properties in our second scenario, the first scenario shows a pronounced increase in ice water path and a noticeable impact on cloud radiative forcing.

Sensitivity studies with the MAECHAM4/CHEM with respect to a variable aerosol concentration

Furthermore sensitivity studies have been performed with the CMCM where only the volcanic radiative effect, only heterogeneous chemistry, or only the impact on the photolysis routine has been considered. Heterogeneous chemistry plays the dominant role in the aerosol containing layers between 20-30 km with increases in the CLOX concentration up to 100% and decreases in the NOX concentration of more than 50%. Aerosol induced heating leads to an uplifting of the trace gases. This results in a decrease in the aerosol containing layers and an increase in the upper stratosphere, which can clearly be seen in the NOX and CH_4 concentrations. The changes in the ozone concentration due to the volcanic aerosol are a combined effect of changes in the photolysis rates, in the heterogeneous chemistry and the heating rates. The tropical O_3 concentration decreases below 30km due to heterogeneous chemistry and upward transport and increases above 3 0km due to a decrease in NOX (Figure WP6-3-3). A detailed investigation of the temperature effects revealed that the temperature anomaly at 50 hPa is largely due the aerosol induced radiative heating (direct effect). Heterogeneous chemistry on the volcanic aerosols particles leads to a temperature decrease of up to –1 k in October 1991 while aerosol induced changes in the photolysis rates have an opposite effect. A publication of the results together with MPI-PROVAM is in preparation.

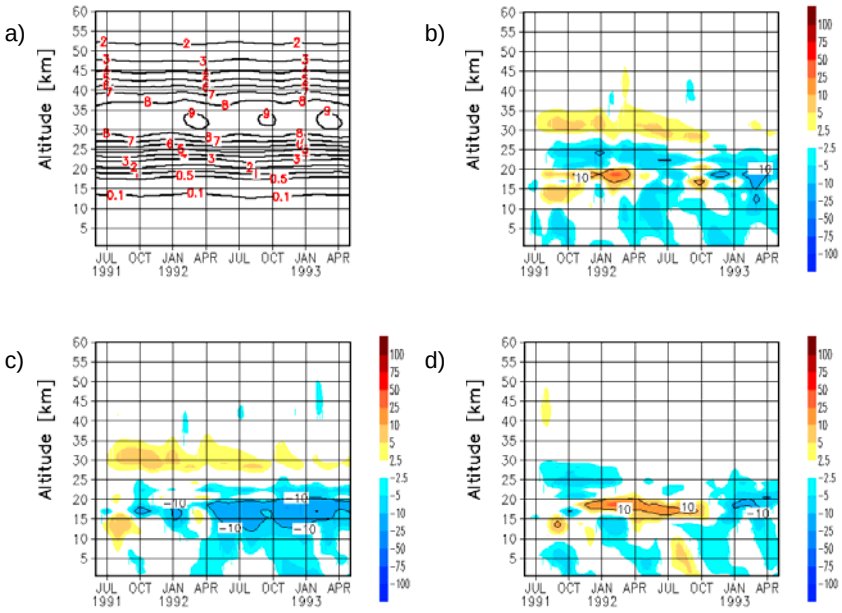

Fig. WP6-3- 3 Relative Ozone Change (%) (tropical average 30°S-30°N) after the Pinatubo eruption a) Control run. b) Effect of all processes. c) Effect of heterogeneous chemistry. d) Effect of radiation.

New publications with contributions from WP6

Lohmann, U., B. Kärcher and C. Timmreck, Impact of the Mt. Pinatubo eruption on cirrus clouds formed by homogeneous freezing in the ECHAM GCM. J. Geophys. Res. 108 (D18),4568,doi:10.1029/20002JD003185, 2003.

Timmreck, C., H.-F. Graf and B. Steil (2003), Aerosol chemistry interactions after the Mt. Pinatubo eruption, in *Volcanism and the Earth's Atmosphere,* eds. A. Robock and C. Oppenheimer, AGU Monograph, 139, p 213-225, 2003.

References

Angell, J. K., Estimated impact of Agung, El Chichon and Pinatubo volcanic eruptions on global and regional total ozone after adjustment for the QBO, Geophys. Res. Lett., **24**, 647-650, 1997.

Luo, B., Z.W.B. Rossow, T. Inoue, and C.J. Stubenrauch, Did the eruption of the Mt. Pinatubo volcano affect cirrus properties?, J. Clim., **15**, 2806-2820, 2002.

Randel, W. J, F. Wu, J. M. Russell III, J. W. Waters, and L. Froidevaux, Ozone and temperature changes in the stratosphere following the eruption of Mount Pinatubo, J. Geophys. Res., 100, 1675316764, 1995.

Wylie, D., W.P. Menzel, H.P. Woolf, and K.I. Strabala, Four years of global cirrus cloud statistics using HIRS, *J. Clim*., 1972-1986, 1994.

Zerefos, C.S., K. Tourpali, and A.F. Bias, Further studies on possible volcanic signal to the ozone layer, *J. Geophys. Res.*, **99**, 25741-25746, 1994.

Contribution of MPI-C

Influence of solar variability: Stratospheric and tropospheric response to enhanced solar UV radiation

The atmospheric response to the 11-year solar cycle was studied using the fully interactive 3- D coupled chemistry- general circulation model MAECHAM with a complete seasonal cycle. The stratosphere-troposphere system shows partly significant response to a realistic solar cycle enhancement of UV-radiation. This response consists of increases in stratospheric ozone and temperature, giving rise to changes in the zonal wind from the stratosphere into the troposphere. Computed changes of stratospheric ozone, temperature and zonal wind are generally in agreement with observed changes between solar minimum and solar maximum. Observed pattern changes of the stratospheric response between early and late winter are approximately reproduced by the model. Our radiative forcing results show that the 11-year solar cycle effect on 20 global mean temperature is negligible, but simulated responses of sea level pressure do suggest that regional effects are probably significant, e.g. by affecting the North Atlantic Oscillation.

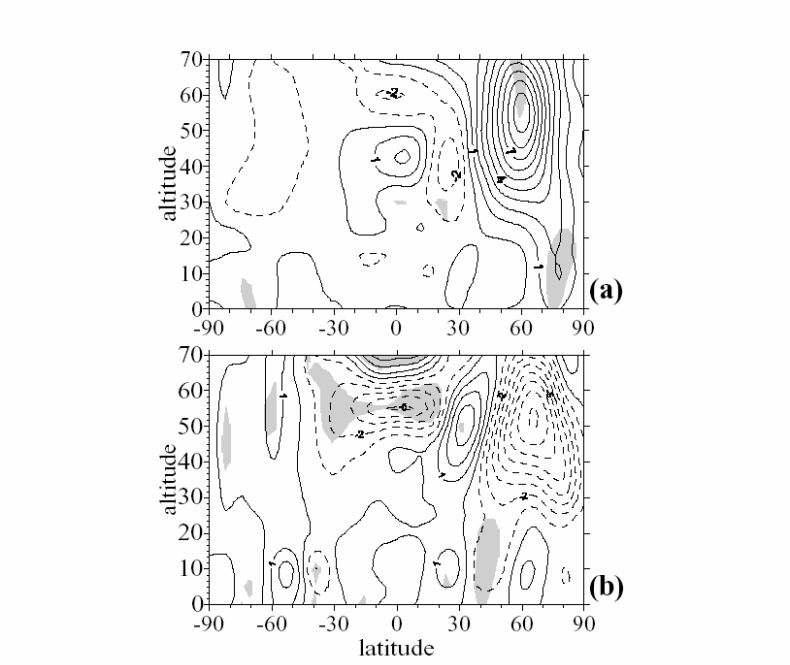

Fig. WP6-4-1: Zonal wind differences (m/sec) for solar maximum relative to solar minimum for (a) December and (b) February. Shading indicates the 95% significance level

New publication with contributions from WP6

K. Tourpali, C. J. E. Schuurmans, R. van Dorland, B. Steil and C. Brühl, Stratospheric and tropospheric response to enhanced solar UV-radiation: a model study. Geophys. Res. Lett., 30, No. 5, 1231, doi:10.1029/2002GL016650, 2003

Contribution of MPI-MAECHAM

QBO: Extension of QBO-assimilation scheme

Introduction

The mean meridional circulation of the middle atmosphere is characterized by upwelling in the tropics and downwelling in the high latitudes, specifically in the winter hemisphere. The so-called Brewer Dobson circulation above the tropopause region is driven mainly by dissipation of waves in the mid and high latitude stratosphere and mesosphere. However, within the tropics the quasi-biennial oscillation (QBO) has a strong impact on the local structure in space and time of the mass transport. This impact consists not only in quasi-biennial variations of the residual circulation (v*,w*) and temperature, but also in a QBO average net effect. This work quantifies the average QBO effect on the residual circulation and temperature in the tropics by comparing two experiments with and without a QBO, respectively.

The QBO has two specific properties which imply a QBO averaged net effect on the residual circulation. Firstly the zonal wind in the QBO has a bimodal distribution in zonal wind speed, and secondly the easterly and westerly phases have different levels of maximum duration (Naujokat, 1986). The easterly phase dominates in the upper levels of the QBO domain while the westerly phase prevails at lower levels. Hence the average of a QBO cycle consists of easterlies and westerlies at upper and lower levels of the QBO domain, respectively. As a consequence the long term average of the secondary meridional circulation of the QBO, which contributes to the general residual circulation, is non-zero as well. Further it follows that the long term average of the observed general circulation in the QBO domain must differ systematically from the long term average obtained from a GCM simulation that does not contain the QBO. The purpose of this work is therefore to quantify this systematic difference by comparison of two experiments which exclude and include, respectively, the QBO. Such an estimate is of interest since GCM experiments often do not include the QBO.

Experiments and Methodology

The following experiments are based on MAECHAM5, the middle atmosphere version of the ECHAM5 GCM. (MA)ECHAM5 is the successor of (MA)ECHAM4 (Roeckner et al., 1996; Manzini et al., 1998).

The GCM resolves the atmosphere from the surface up to 0.01 hPa (ca. 80 km). While the standard middle atmosphere model uses 39 layers (L39), the model simulating the QBO resolves the atmosphere with 90 layers (L90). The horizontal resolution is T42.

Two experiments L39 and L90 are run with climatological boundary conditions for sea surface temperature and sea ice. The control experiment L39 has no QBO, thus corresponds to the majority of GCM experiments concerning the absence of the QBO. Experiment L90 differs from L39 in the improved vertical resolution only. As a result the QBO is generated spontaneously (Giorgetta et al., 2002).

For the following analysis it is useful to separate a variable X within the QBO domain in the following components:

X(t) = Xc + Xa(t) + Xr(t)
Xc = climatological annual mean of X
Xa(t) = climatological annual cycle
Xr(t) = residual part

The Xa component is strictly periodic, with a one year period by construction, and contains the annual, semi-annual and higher harmonics. The Xr component includes the QBO variation, the dominant portion of variability in the QBO domain, and other components, either non-periodic or periodic. For

the following analysis the Xc components of both experiments are used to define the average QBO effect:

XcQBO = Xc(L90)-Xc(L39)

Results

The average QBO effects in U and w*, averaged from 10°N to 10°S, are shown in Figure WP6-5-1 for U and w*. The profile of U_c(L39) (Figure WP6-5-1a) has one broad minimum (-10 m/s) near 40 hPa without any further structure. The profile U_c(L90), however, shows a maximum (-1 m/s) near 45 hPa and a minimum (-15 m/s) near 17 hPa, as anticipated from the prevalence of QBO easterlies and westerlies in the upper and lower levels of the QBO domain. The difference U_cQBO of both profiles (Figure WP6-5-1 b) shows a maximum of +9 m/s near 40 hPa and a minimum of -9 m/s near 20 hPa, both significant at the 95% level.

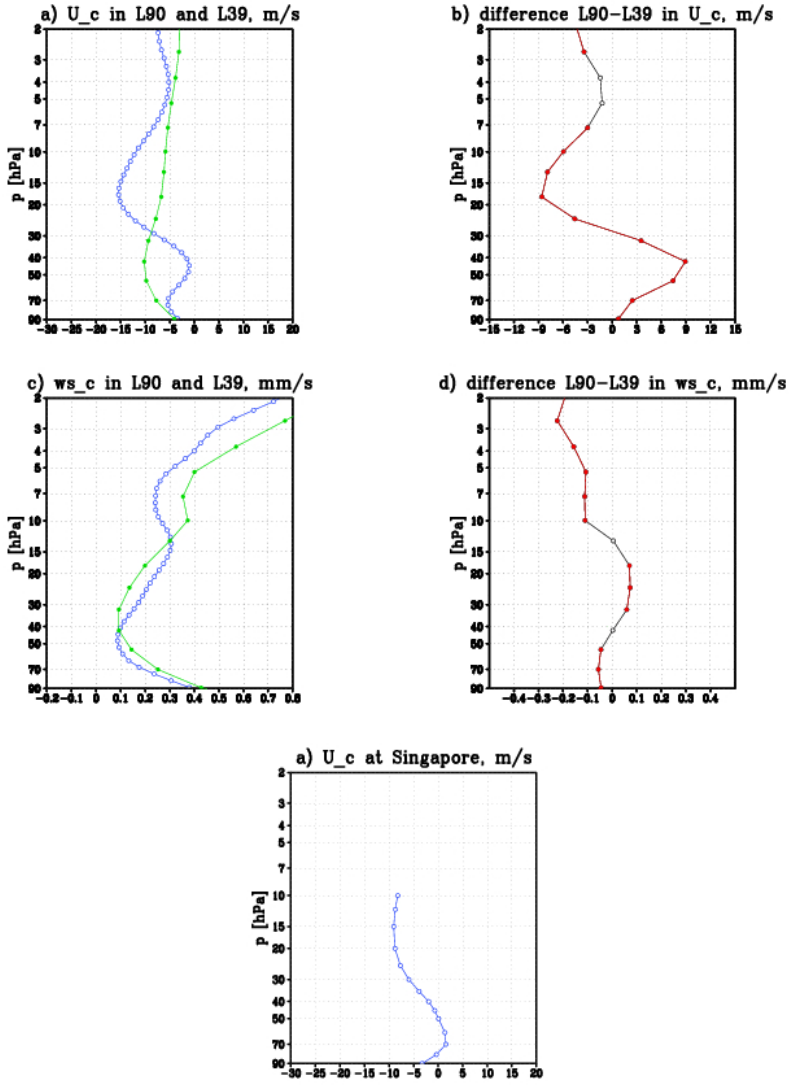

Fig. WP6-5-1: a) Climatological zonal mean zonal wind U_c (m/s) in L39 (green) and L90 (blue), b) difference of U_c in L90 and L39, significant differences (95%) are shown in red; c) and d) analogous to a) and b), respectively, for w*c (mm/s); e) climatological zonal wind U_c (m/s) at Singapore 1971-2000.

As a consequence, the long term average of the secondary meridional circulation of the QBO is non-zero as well. The vertical component w*c averaged from 10°N to 10°S is shown in Figures WP6-5-1c for both experiments. In L90, w*c is reduced (increased) below (above) 40 hPa with respect to w*c in L39 (40 hPa is the position of the maximum in U_cQBO). The minimum in w*c is 0.1 mm/s in both

experiments, though the levels of the minimum are different: 35 hPa in L39 and 45 hPa in L90.Comparing the time mean profile in U_c at Singapore (Figure WP6-5-1e) and U_c in the L90 profile (Figure WP6-5-1 a) one finds qualitative agreement in the shape of the profiles, and agreement in the position of the minimum near 15 hPa. The position of the maximum is too high in the simulation. The amplitudes differ to some degree which is explained in part by the local character of the observed wind.

The integral effect of the QBO on the long term mass flux has consequences for the duration spent by upwelling air parcels in the equatorial stratosphere. Figure WP6-5-2 compares the time series of the annual variation in equatorial specific moisture, the so-called atmospheric tape recorder (ATR) (Mote et al., 1996), averaged from 10°N to 10°S. The ascent of a minimum or maximum from 90 hPa to 10 hPa takes 17 months in experiment L90, in good agreement with the estimates in Mote et al. (1996), but only 12 months in experiment L39, where the QBO is missing entirely.

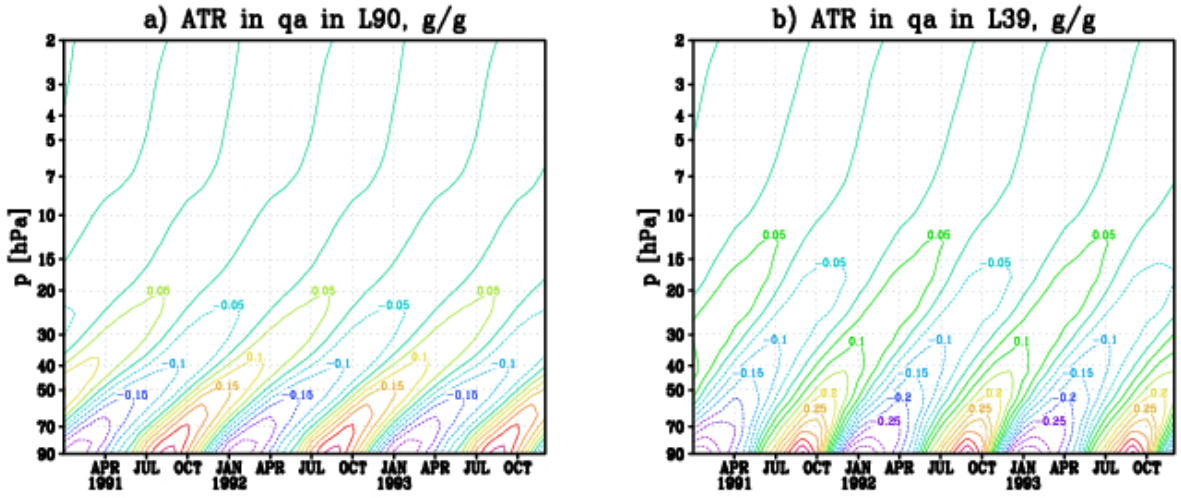

Fig. WP6-5-2: a) Atmospheric tape recorder in specific humidity qa (ppmv) in L90, b) in L39.

Conclusions

The QBO has a net effect on the climatological annual means of variables in the QBO domain. Neglecting the QBO in GCM simulations necessarily results in systematic biases in zonal wind, residual meridional circulation, temperature, and residence time in the lower tropical stratosphere. The QBO and its effects cannot be removed from observed time series by temporal averaging over full QBO cycles. Hence it is necessary to include the QBO in GCM based studies of the tropical stratosphere, either by direct simulation, as used here, or by assimilation as chosen for the KODYACS transient experiments where the QBO evolution is known. Including the QBO specifically improves the upwelling in the tropical lower stratosphere as evident in the simulated atmospheric tape recorder in specific humidity.

Sensitivity of the QBO simulated in MAECHAM5 to climate change

The QBO is an important factor for the explanation of the observed inter-annual variability of the dynamics and trace gas concentrations in the stratosphere (*Steinbrecht et al.*, 2003). For this reason it has been decided to include the observed QBO in the transient chemistry climate simulations for the period 1960 to 2000, as carried out in the KODYACS project. For the prediction of future climates including the composition of the atmosphere it is hence very desirable to include the QBO effects on transport and chemistry as well, which requires, however, to investigate first the properties of the QBO in a future climate. For this purpose a set of experiments has been devised to investigate the QBO in a $2xCO_2$ climate. These experiments make use of the MAECHAM5 GCM, which simulates a realistic QBO for current climate conditions (*Giorgetta et al.*, 2002), which depends on the models ability to represent a realistic spectrum of tropical precipitation (*Horinouchi et al.*, 2003). The set of

experiments includes a 30 year QBO simulation for current climatological sea surface temperature (AMIP2) and CO_2 concentration (348 ppmv), and three 10 year integrations with climatological lower boundary conditions representative for a $2xCO_2$ climate (696 ppmv). The $2xCO_2$ experiments differ from each other by the source strength of the gravity wave spectrum launched in the troposphere. These source level are increased by 0%, 10%, and 20%, respectively, compared to the control experiment. A preliminary evaluation of these experiments (*Doege*, 2003) shows, that the QBO will accelerate its frequency in a significant manner with average periods of 26, 22, and 17 months, respectively. The potential transport effects on the trace gases still have to be assessed.

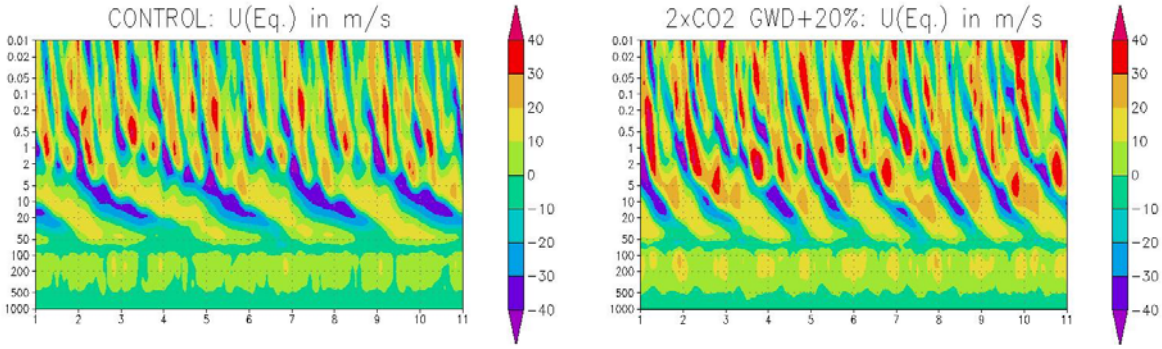

Figure WP6-5-3: QBO simulated for current climate (left) and QBO simulated for $2xCO_2$ conditions and 20% increased gravity wave forcing. Both panels show the zonally averaged zonal wind at the equator.

New publication with contributions from WP6

Giorgetta, M. A., E. Manzini, and E. Roeckner, Forcing of the quasi-biennial oscillation from a broad spectrum of atmospheric waves. *Geophys. Res. Lett.*, 29, 10.1029/2002GL014756, 2002.

References

Manzini E., and N. A. McFarlane N.A., The effect of varying the source spectrum of a gravity wave parameterization in a middle atmosphere general circulation model. J. Geophys. Res., 103, 31523-31539, 1998.

Mote, P. W., K. H. Rosenlof, M. E. McIntyre, E. S. Carr, J. C. Gille, J. R. Holton, J. S. Kinnersley, H. C. Pumphrey, J. M. Russel III, and J. W. Waters, An atmospheric tape recorder: The imprint of tropical tropopause temperature on stratospheric water vapor. *J. Geophys. Res.*, 101, 3989-4006, 1996.

Naujokat, B., 1986: An update of the observed quasi-biennial oscillation of the stratospheric winds over the tropics. *J. Atmos. Sci.*, 43, 1873-1877, 1986.

Roeckner, E., K. Arpe, L. Bengtsson, M. Christoph, M. Claussen, L. Dümenil, M. Esch, M. Giorgetta, U. Schlese, U. Schulzweida, 1996: The atmospheric general circulation model ECHAM4: Model description and simulation of present-day climate, MPI Rep., 218, Hamburg, Germany, 1996.

Natural forcing in CCM transient runs

For the first time, transient simulations have been carried out (DLR, MPI-MAECHAM, MPI-C), which have considered major components of natural forcing: The quasi-biennial oscillation (QBO), the 11-year solar activity cycle, and major volcanic eruptions.

Contribution by MPI-MAECHAM and MPI-C

Studies with the CCM MAECHAM/CHEM

The CCM MAECHAM4/CHEM has been integrated for 40 years (1960-1999) in transient mode with forcings from the 11 year solar cycle (UV-radiation), the 3 major volcanoes Agung, El Chichon and Pinatubo, assimilated Quasi-Biennial Oscillation (QBO, Giorgetta and Bengtson, 1999), and the transient observed sea surface temperatures of Hadley Centre. The varying UV-radiation due to the 11 year solar cycle has its large impact in the mesosphere and the upper stratosphere. Because of enhanced photolysis in the Lyman-alpha-region water vapour is reduced there at solar maximum. On the other hand at solar maximum ozone production by photolysis of oxygen is enhanced. Both effects lead to enhanced ozone in the upper stratosphere for solar maximum (Figure WP6-6-1, 0.2ppmv), accompanied by heating, and reduced ozone for solar minimum especially in the tropics, which is also visible in total ozone. In the tropics the largest modulation of lower stratospheric ozone and total ozone is exerted by the QBO. In Figure WP6-6-1 in the westerly QBO phase equatorial ozone is enhanced compared to the eastphase (opposite in the subtropics). The typical variation in total ozone is about +/-8DU (or +/-0.3ppmv locally in Figure WP6-6-1). Transport effects on ozone are enhanced via the modification of odd nitrogen which acts as ozone source in the lower stratosphere and a catalytic sink above about 30km. This behaviour change is reflected in a sign change in the ozone anomalies with altitude. The QBO related changes in the residual vertical wind lead to temperature changes in the order of +/-5K. The major volcanoes have in this model the largest effect via enhanced water vapour by heating of the tropopause region and enhanced ozone depletion by odd hydrogen (up to 10DU). Also shown is the heterogeneous removal of reactive nitrogen in the middle and lower stratosphere by the aerosol of the eruptions of Agung, El Chichon and Pinatubo. This leads also to a reduced ozone production amplifying the reduction related to enhanced HO_x chemistry. In the tropical tropopause region in La Nina years NO_x and ozone are enhanced, in El Nino years slightly reduced. Fig WP6-6-1 shows also the trend in ozone and temperature in the upper stratosphere related to CFC-and CO_2 increase in agreement with observations.

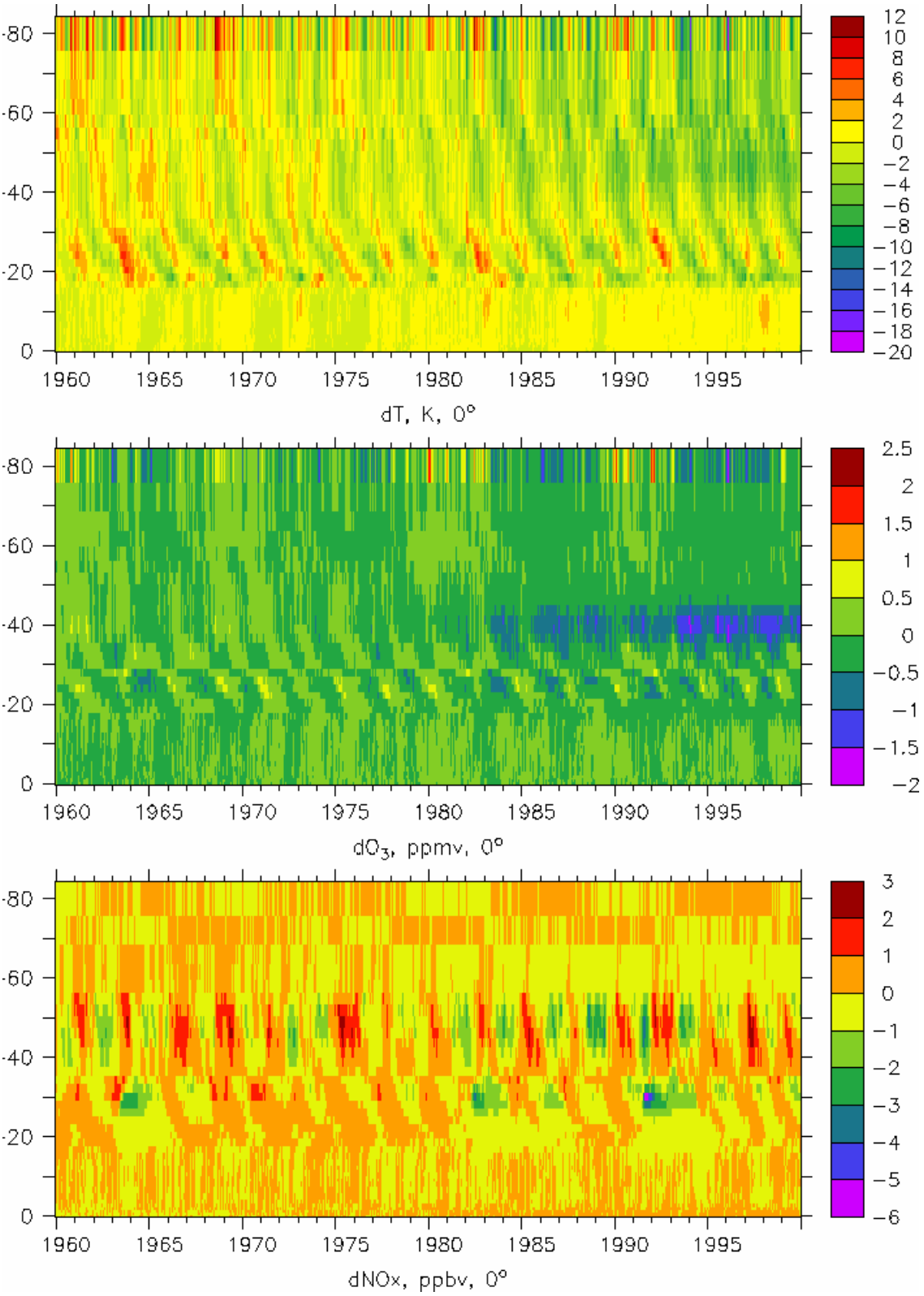

Figure WP6-6-1: Temperature, ozone, and NO_x anomalies in a 40 years transient simulation with MAECHAM/ CHEM at the equator. The average seasonal cycle of the first 20 years is subtracted, data given as 10-day, zonal averages. Vertical axis is pressure altitude.

Contribution of DLR

Investigation of impacts of natural forcing in the CCM E39/C

For the transient simulations with E39/C (1960-1999; see also WPs 1, 3, 4, and 5) the QBO has been adapted ("nudged") to observed lower stratosphere zonal winds near the equator (ECMWF-analyses), influences of solar activity changes as well as impacts of volcanic eruptions have been considered in radiative transfer (heating rate) calculations and the chemistry module, respectively.

A modulation of dynamic and chemical quantities caused by the prescribed QBO is manifoldly found in the model data. For example, in Figure WP6-6-2 a QBO signal can clearly be identified by eye in the equatorial region. Qualitatively, it is in good agreement with a similar analysis derived from a merged satellite data set and ground based data, respectively (Bojkov and Fioletov, 1995; updated version until the year 2000 is to our's disposal, Fioletov, pers. communication; see also Figure WP4-3). Whereas the anomalies in observations and the model results are of the same order of magnitude until the 1980s (i.e. up to 6%), they are obviously smaller during the 1990s in E39/C, where observed fluctuations have continued with similar magnitudes, but the modelled ozone varies only by about 2-3%. The QBO signal in E39/C can be detected in total ozone in all latitudinal regions. For example, at mid-latitudes of the Northern Hemisphere (Figure WP6-6-3) E39/C results show amplitudes in total ozone of 12DU ± 4DU during winter months (JFM) which can be clearly related to the QBO. Similar results have been found in an analysis based on TOMS data (Burrows et al., 2000; see also figure 2.4 in EC-report, 2001). A linear regression analysis of long-term measurements of ozone at Hohenpeissenberg (47°N) indicates QBO-related fluctuations of ±10DU (peak-to-trough ozone changes up to 20DU) in February (Steinbrecht et al., 2001; see also WP1).

The impact of solar activity, in particular of the 11-year solar cycle, on the stratosphere has often been investigated. For example, total ozone anomalies have been estimated in the tropics (25°N to 25°S) for the years from 1978 to 2003 (WMO, 2003; Figure 4-5 therein). This analysis was made on the basis of different observations (synergistic use of ground based and satellite data). It clearly shows strong decadal variations of total ozone in the tropics (approx. 3%), which indicates the link between long-term ozone changes especially in tropical regions and the activity cycle of the sun. Calculated ozone anomalies derived from E39/C (Figure WP6-6-2) are very similar, with positive anomalies around solar maximum (1980 and 1991) and minimum anomalies around solar minimum (1986 and 1996). Model data for the years before 1978 seems to indicate a likewise behaviour, with higher ozone values around 1960 and 1970 (maximum solar activity) than around the year 1965 (minimum solar activity).

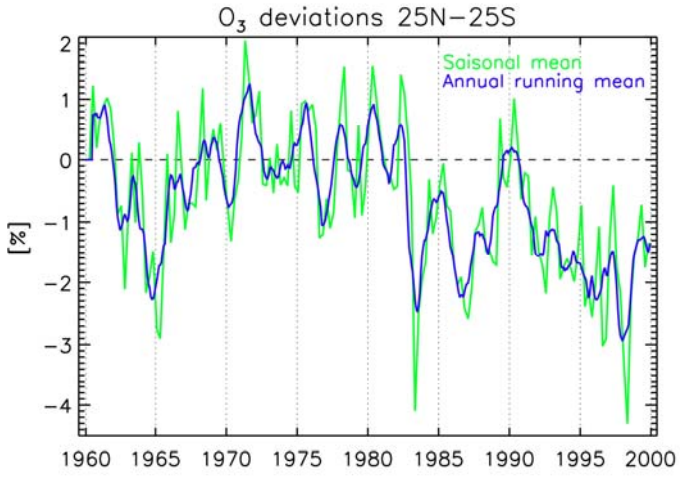

Figure WP6-6-2: Mean relative ozone anomalies derived from E39/C, calculated for the latitudinal region between 25°N and 25°S; seasonal and annual running mean values are calculated with respect to data between 1964 and 1980.

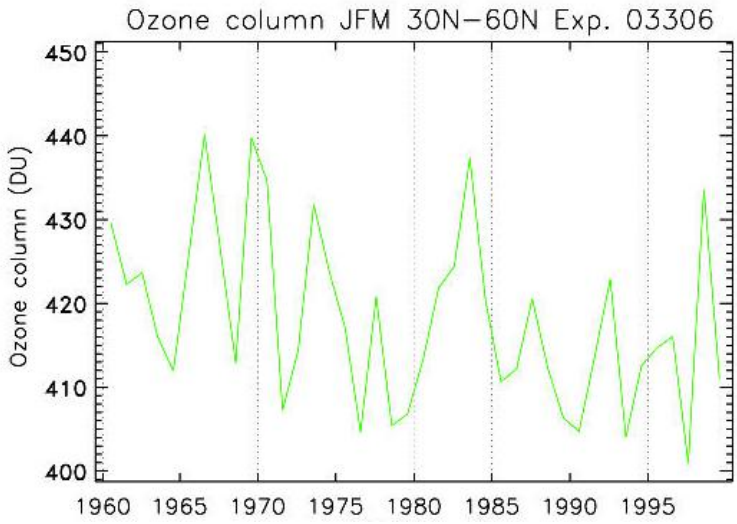

Figure WP6-6-3: Variability of the mean ozone column derived from E39/C transient simulation for middle latitudes of the Northern Hemisphere (30° to 60°N) for the months January, February and March. In Dobson Units (DU).

References:

Burrows, J.P., J. Gleason, G. Labow, K.-U. Eichmann, K. Bramstedt, and M. Weber, An overview of the stratosphere 1995-1999 as measured by GOME, Stratospheric Ozone 1999, Proceedings of the fifth European symposium, N.R.P. Harris, M. Guirlet, G.T. Amanatidis (Eds.), 27 September - 1 October 1999, Saint Jean de Luz, France, Air Pollution Research Report no. 73, EUR 19340, ISBN 92-827-5672-6, 2000.

EC-report, European research in the stratosphere 1996-2000, Advances in our understanding of the ozone layer during THESEO, EUR 19867, ISBN 92-894-1398-0, 378p., 2001.

Giorgetta, M. A. and L. Bengtsson, The potential role of the quasi-biennial oscillation in the stratosphere-troposphere exchange as found in water vapour in general circulation model experiments, J. Geophys. Res., 104, 6003-6019, 1999.

Steil, B., et al, The impact of CFCs, greenhouse gases, solar cycle, QBO, ENSO and major volcanoes on stratospheric ozone; transient simulation with the middle atmosphere coupled chemistry climate model ECHAM for the last 40 years. Proceedings Quadrennial Ozone Symposium, Kos, Greece, 2004.

Steinbrecht, W., H. Claude, U. Köhler, and P. Winkler, Interannual changes of total ozone and northern hemisphere circulation patterns, Geophys. Res. Lett., 28, 1191-1194, 2001.

WMO (World Meteorological Organisation), Scientific Assessment of Ozone Depletion: 2002, Global Ozone Research and Monitoring Project, Report No. 47, 498p., 2003.